Desalination and Water Treatment
www.deswater.com

doi:10.5004/dwt.2017.21578

98 (2017) 196–215
December

Adsorption and photocatalysis activity of TiO_2/bentonite composites

Mounir Kassir[a,b,c], Thibault Roques-Carmes[d,*], Manuel Pelletier[a], Isabelle Bihannic[a], Halima Alem[e], Tayssir Hamieh[b], Joumana Toufaily[b], Frédéric Villiéras[a]

[a]*Université de Lorraine, Laboratoire Interdisciplinaire des Environnements Continentaux, UMR 7360 CNRS, 54500 Vandœuvre-lès-Nancy, France, email: kassirk@hotmail.com (M. Kassir), manuel.pelletier@univ-lorraine.fr (M. Pelletier), isabelle.bihannic@univ-lorraine.fr (I. Bihannic), frederic.villieras@univ-lorraine.fr (F. Villiéras)*
[b]*Laboratory of Materials, Catalysis, Environment and Analytical Methods, Faculty of Sciences I, Lebanese University, Campus Rafic Hariri, Beyrouth, Lebanon, email: tayssir.hamieh@ul.edu.lb (T. Hamieh), joumana.toufaily@ul.edu.lb (J. Toufaily)*
[c]*Plateforme de Recherche et d'Analyse en Sciences de l'Environnement (PRASE), Ecole Doctorale de Sciences et Technologies, Université Libanaise, Campus Rafic Hariri, Beyrouth, Lebanon*
[d]*Université de Lorraine, Laboratoire Réactions et Génie des Procédés, UMR 7274 CNRS, 54000 Nancy, France, email: thibault.roques-carmes@univ-lorraine.fr (T. Roques-Carmes)*
[e]*Université de Lorraine, Institut Jean Lamour, UMR 7198 CNRS, 54011 Nancy, France, email: halima.alem@univ-lorraine.fr (H. Alem)*

Received 30 January 2017; Accepted 22 October 2017

ABSTRACT

This paper explores the impact of the TiO_2 nature and concentration immobilized onto bentonite clay on the adsorption and the photocatalytic degradation of methyl orange and salicylic acid at pH 3 and 10. Commercial P25 TiO_2 and nanoparticles prepared via the sol-gel method have been deposited onto the clay. We paid particularly close attention to the quantitative determination of the TiO_2 content deposited onto the clay from the analysis of the XRD patterns using a Rietveld-based fitting method. The TiO_2 particles play the major role on the photochemical activity and on the formation of the hydroxyl radicals. The constant rate of degradation increases linearly with the titania content immobilized onto the clay. The pollutant removal proceeds more favorably with bentonites containing mixed rutile and anatase crystallographic phases TiO_2 (P25) than with pure anatase sol-gel titanium dioxide. The photodegradation performances are also affected by the adsorption capacity of the clay. When the adsorption of the pollutant remains weak (at basic pH), the bentonite plays no role in the degradation activity. At the same TiO_2 content, the photocatalytic efficiencies of the unsupported and immobilized titania are equivalent. Conversely, at acidic pH the contaminant adsorption becomes significant and all the composites produce the complete degradation of the pollutants. The immobilization of the titania leads to a reduction of the time necessary to remove the contaminants through the enrichment by adsorption of the pollutant onto the clay. The fastest photodegradation is achieved with the composite containing the smallest amount of titania (57 wt.%) but with the largest uptake of pollutant adsorbed.

Keywords: Photocatalysis; TiO_2/clay composite; Bentonite; Titanium dioxide; Rietveld method

1. Introduction

Environmental concerns such as water quality have attracted considerable attentions. There are an increasing number of studies on the development of efficient wastewater treatments. Heterogeneous photocatalysis appears as an interesting alternative method because it offers several advantages compared to the classical processes (adsorption, chemical treatment, etc.) [1–3]. Up until now, titanium dioxide remains the mostly used photocatalyst for the degradation of organic pollutants from wastewaters [4–7]. A major issue when using TiO_2 nanoparticles is the low stabil-

*Corresponding author.

ity of the suspensions. Actually, the powders agglomerate into larger aggregates [8–10]. This coalescence produces a significant diminution of the available catalyst surface for the light and the pollutants. Consequently, it reduces the contaminant adsorbed amount and the light absorption.

In an attempt to overcome the TiO_2 aggregation, it becomes clear that the immobilization of the titania photocatalyst on a convenient support could be advantageous [11–13]. Clays appear as interesting supports for TiO_2 owing to their low cost and large adsorption capacity [14,15]. Accordingly, clay minerals impregnated with TiO_2 lead to enhanced pollutants incorporation and diffusion owing to large pore size. As a matter of fact, the clays display no photocatalytic activity while they produce an enhancement of the surface contact for the photocatalysis reaction [14,15]. Several clays have been already tested to immobilize the titania. Bentonite [14–16], sepiolite [17,18], montmorillonite [19], kaolinite[20–22] and stevensite [23] are some examples. In general, the photocatalytic efficiency of TiO_2/clay systems is greater as compared to pure TiO_2 samples.

Among the methods used to prepare TiO_2/clay composites, the sol-gel approach remains the most widely used [15,18,19,21,24,25]. This way to synthesize titania leads to a better control of the deposition of the nanoparticles onto the clay but it presents the disadvantage to produce pure anatase titania after calcination. However, several studies have demonstrated that titania nanoparticles with mixed anatase and rutile crystallographic phases (such as the commercial P25 photocatalyst) possess better photochemical activity than that of pure anatase TiO_2 [6,26,27]. For that reason, it appears interesting to investigate the photocatalytic performances of P25 TiO_2 immobilized onto clay. Its photocatalytic activity will be logically compared to the titania system prepared via the classical sol-gel route. The photocatalytic degradation of methyl orange and salicylic acid aqueous solutions at different pH are used as probe reactions. We have identified bentonite as valuable support due to the high photocatalytic performances of the TiO_2/bentonite systems [14,15]. In addition, this lamellar crude mineral remains cheap and widely used in wastewater treatment as adsorbent. Generally, the layer structure of this material is composed of two silica tetrahedral sheets fused to one alumina octahedral sheet. The main novelty of our work concerns the development of a relationship between the TiO_2 content immobilized onto the clay, the titania nature (crystallographic nature), the TiO_2 packing onto the bentonite, the pollutant adsorbed amounts onto the composite, and the photodegradation performances of the titania/bentonite systems. Despite TiO_2/bentonite is somewhat classical system, this is the first time that this kind of comprehensive and detailed study is applied to this material.

However, for a better understanding and analysis of the photocatalytic data using the various titania/bentonite systems, a knowledge of the TiO_2content deposited onto the clay is required. In this context, several methods can be used to provide valuable information on the titania uptakes immobilized onto the clay. Elemental analysis using X-ray fluorescence spectrometry (XRF) is the most traditionally used analysis technique [18,24,28]. Inductive coupled plasma-optical emission spectroscopy [21] and X-ray photoelectron spectrometry [25] can be also employed. In this paper, we propose to use an alternative method based on a Rietveld fitting of the X-ray powder diffraction patterns. Actually, X-ray powder diffraction coupled with a Rietveld analysis appears as a very powerful method for the accurate estimation of the phases proportion from multicomponent mixtures [29–34].

2. Materials and methods

2.1. Materials

Two kinds of TiO_2 nanoparticles were used. Titanium dioxide powder P25 was employed since it remained the state of the art photocatalyst [1,3–5]. It was supplied by Evonik-Degussa. The particle diameter, estimated by transmission electron microscopy (TEM), was about 25–30 nm. Titania prepared by the sol-gel process was also investigated. The sol-gel precursor was titanium isopropoxide (IPPT, 99.8%) from Sigma Aldrich. Acetic acid (98.9%) supplied by Sigma Aldrich was employed during the synthesis.

The natural bentonite clay came from Georgia (Europe) and was provided by the company IKO (IBECO, S&B Industrial Minerals GmbH). The material contained more than 70% of swelling montmorillonite and also other minerals including muscovite, quartz, calcite, dolomite, cristobalite and albite. The cation exchange capacity (CEC), estimated with Na^+ as exchangeable cation, amounted to 95.5 meq/100 g of dry matter.

2.2. Samples preparation

Two methods were applied to prepare the bentonite supported titania particles. The first route employed commercial titania P25 as photocatalyst. Initially 100 mL of TiO_2 P25 colloidal aqueous dispersion was prepared. The weight of TiO_2 was varied from 0.3 g to 4.5 g. The solution pH was adjusted to 1.5 by adding 0.1 M HCl solution drop wise. In parallel, the bentonite was suspended in water (1 g of powder in 100 mL) and the suspension was kept at room temperature for 24 h to swell the clay. After completion of these steps, the positively charged TiO_2 particles were then coagulated with the negatively charged clay layers (see Fig. S1 of the Supporting information). For this purpose, the TiO_2 colloidal solution was added dropwise into the clay suspension under vigorous stirring. After 12 h of stirring at room temperature, the reaction was stopped. The suspension was centrifuged. Then, the precipitate was thoroughly washed with distilled water, dried at room temperature for 24 h, and finally calcinated at 450°C for 4 h under an ambient atmosphere. The resultant samples were named as P25 titania/bentonite composites.

For the other preparation method, the titania was synthetized by the sol-gel technique. The composites were prepared by following the procedure reported by Kitayama et al. [35]. A TiO_2 sol stock dispersion was first prepared. For this purpose, a given mass of titanium tetraisopropoxide (IPPT) was added to a vigorously stirred 80 wt.% acetic acid solution which contained 5 mL of water and 20 mL of acetic acid. To modulate the titania amount, the IPPT initial masses were scaled in the range of 1–16 g. The mixture was magnetically stirred at 50°C for 40 min to obtain the transparent sol [36,37]. In parallel, the bentonite was dispersed in water (1 wt.%) and was maintained under stirring at room

temperature during 24 h. After that period, the titanium sol solution was mixed with the clay aqueous suspension. The final mixture was then stirred for 2 h at room temperature. The resulting suspension was separated and centrifuged two times at 7000 g. The powder was dried under dry air at room temperature, and then calcinated at 450°C for 4 h. The as-synthetized bentonite supported titania were denoted as sol-gel titania/bentonite.

The absence of TiO_2 leaching from the clay was studied. For this purpose, the calcined composites were redispersed in pure water and maintained under magnetic stirring for 3 h. At the end of the rinsing step, the samples were centrifuged at 3000 rpm for 6 min in order to separate the composites from the supernatant. The centrifugation was not able to separate the non-attached titania from the solution. The possible presence of titania in the supernatant (leached) was monitored by means of both turbidimetric analysis (estimated by the transmission of light, ratio of transmitted light intensity: $T = I/I_0$) and UV/visible spectroscopy measurements. For all the samples, the large transmittance (0.98–0.99) in turbidimetry and the insignificant absorbance detected between 300 and 400 nm (UV/vis spectroscopy) indicated the absence of TiO_2 leaching from the clay or, at least, a very low removing of titania after 3 h in water (Figs. S2 and S3 of the Supporting information S2). In order to ensure that TiO_2 leaching from the clay can be neglected and that the titania deposited onto the bentonite remained constant throughout the photocatalytic process, the duration of each experiment was carefully limited to 3 h (1 h of adsorption in the dark and 2 h under illumination).

2.3. XRD measurements and quantification of TiO_2 content

Powder X-ray diffraction (XRD) measurements were recorded by means of a D8 Discover BRUKER diffractometer. The apparatus employed CuKα or CoKα radiations. The samples were prepared in plastic holders where the powders were poured and flattened using a glass slide. The samples were scanned from 3 to 64° (2θ) using steps of 0.04° and a counting time per step of 8 s.

The quantitative crystallographic phase analysis was carried out using TOPAS 4.2 software (Bruker). The program consisted in a graphics based profile built around a general non-linear least square fitting system of experimental diffraction pattern. Among the various types of profile fit methods available, the fit was achieved through the Rietveld strategy. The latter process was based on the adjustment of the crystal structures, *i.e.* the crystallographic parameters used in the calculation of a diffraction pattern, to those obtained experimentally from X-ray diffraction. The simulated XRD pattern was estimated based on a large number of parameters, including such concerning the crystal-structure of each component phase, those describing the peak profile and the background, those simulating the instrumental aberrations as well as a scale factor which was necessary to adjust the relative intensities of the reflections. The method has been described previously by our group [38] and is also given in the Supporting information S3. Actually, the method was mainly used for the estimation of the weight percentage of TiO_2 nanoparticles deposited onto the bentonite. All the crystallographic phases, except those of titania (rutile and anatase), were considered to belong to the clay. The weight percentage of titania was obtained from the proportion of anatase, rutile and clay.

To validate the quantitative crystallographic phase analysis, the titania contents were also measured by X-ray fluorescence spectroscopy (XRF). For the P25 titania/bentonite materials, the XRF analyses were conducted with initial masses of catalyst in solution of 50 and 82 wt.% (relative to the mass of bentonite). For the sol-gel titania/bentonite materials, the measurements were conducted with initial masses of titanium tetraisopropoxide (IPPT) of 10 and 17 wt.% (relative to the mass of water).

2.4. Characterization of the TiO_2/bentonite composites

In addition to the XRD analysis, other techniques were employed to thoroughly characterize the bentonite supported TiO_2 particles systems. The morphology of the composites was monitored by transmission electron microscopy. TEM imaging was performed by placing a drop of the particles in ethanol onto a carbon-coated copper grid. Samples were studied by using a Philips CM20 instrument with LaB_6 cathode operating at 200 kV. The nitrogen adsorption-desorption isotherms were recorded, at 77 K, on a Micromeritics TRISTAR 3000 instrument. The specific surface area was evaluated by applying the Brunauer-Emmet-Teller (BET) equation to the adsorption data. Ultraviolet-visible (UV/vis) diffuse reflectance spectra were obtained using a UV/vis spectrophotometer (Shimadzu). The solid sample (10 wt. %) was mixed with dry $BaSO_4$.

2.5. Photocatalytic activity of TiO_2/bentonite composites

The adsorption coupled to the photocatalytic efficiency of the TiO_2/bentonite composites were evaluated towards the degradation of methyl orange and salicylic acid. To this purpose, the analyses were carried out, at room temperature, in a reactor which consisted of a glass Petri dish. The latter had an internal diameter of 5.8 cm and a volume of 100 mL. A mercury lamp (low pressure mercury arc) emitting in the near-UV was above the reactor. The artificial light was put outside the reactor and was parallel to it. The intensity of the UV radiation at the top of the dispersion amounted to 10^{-6} Einstein L^{-1} s^{-1}.

The adsorption and the photocatalytic experiments were conducted in aqueous suspensions of catalysts containing the pollutant. The solid loading was fixed to 1 g/L while the initial contaminant concentration (methyl orange or salicylic acid) was adjusted to 10 mg/L. The volume of the suspensions was 80 mL. The pH of the suspensions was fixed to pH 3 or 10 by adding dropwise concentrated solutions of HCl or NaOH, respectively. In a typical experiment, the suspension containing the pollutant was kept under magnetic stirring in the dark during 1 h. This step appeared necessary to ensure the adsorption/desorption equilibrium [7]. After completion of this step, the lamp was switched on and the irradiation of the suspension was carried out under continuous magnetic stirring. At defined time intervals, about 3 mL of the irradiated suspensions were collected by means of a syringe, and then filtrated using a 0.1 μm filter (PTFE Millipore) to remove the particles from the solution. Note that, at the end of the dark adsorption period (irradiation time = 0), a sample was withdrawn in order to evaluate the

adsorption capacity of the catalyst. The methyl orange concentrations were determined by recording the absorbance of the solutions, at a wavelength fixed at 458 nm, using a UV/visible spectrophotometer. The concentration of salicylic acid was estimated using standard calibration curve at 295 nm. In order to evaluate the mineralization of the contaminants, the total organic carbon (TOC) of the withdrawal liquids was also analyzed by the means of a Shimadzu carbon analyzer (TOC-5000A). The initial bulk TOC were equivalent to 15.6 mg carbon/L and 16.3 mg carbon/L for methyl orange and salicylic acid solutions, respectively.

It is now well established that the photocatalytic data can differ from one run to another. In the present study, for each material and condition, every experiment was repeated three times to obtain reliable results. The data presented in the figures (bulk concentration vs. irradiation time) were the averages of the repeated results. It appeared also necessary to perform blank experiments under the same conditions. The photolysis of methyl orange and salicylic acid can be neglected (not shown), while the raw bentonite did not produce methyl orange and salicylic acid degradation under UV light irradiation (Fig. S11 of the Supporting information S4). This confirmed that the bentonite displayed no photocatalytic activity.

3. Results and discussions

3.1. Quantification of TiO_2 content using XRD measurements

The influence of the initial mass of P25 titania (Fig. 1A) and titanium tetraisopropoxide IPPT (Fig. 1B) on the X-ray diffraction patterns of TiO_2/bentonite samples is depicted in Fig. 1.The X-ray diffraction patterns are plotted within the 2θ range from 15°to 30° since the Rietveld analysis is performed with the same 2θ values.

For all the composites, the reflection related to the bentonite clay is observed at 2θ = 19.7° ("Mo"). Note that the peak situated at 2θ = 26.8° belongs to the quartz impurities of the bentonite. The peak located at 2θ = 25.4° ("An"), which belongs to the anatase phase of titania, is evidenced regardless of the titania precursor. This confirms the presence of titania onto the clay for all the mixtures. For the P25 TiO_2/bentonite composites, the peak corresponding to the rutile phase of titania appears at 2θ = 27.4° ("R"). Conversely, the absence of this peak for the samples prepared via the sol-gel method, emphasizes that anatase is the only formed crystalline phase. Upon the addition of titania P25 or IPPT sol-gel precursor, the intensity of the peak of the bentonite progressively decreases while the intensity of the anatase peak is enhanced. As far as the sol-gel titania/bentonite composites are concerned, it is interesting to discuss the link between the degree of crystallinity of the anatase phase and the amount of IPPT precursor. Untilan initial mass of IPPT of 6 g, a poor anatase crystallinity is detected. For larger IPPT contents, a high crystallinity becomes apparent.

The XRD diffraction patterns can also be employed to obtain information about the mean TiO_2 crystallite size. Calculations using Scherrer formula point out a significant difference in the titania crystallite size between the P25 containing samples and the sol-gel prepared composites. The TiO_2 crystallite size of the P25 containing samples range between 19 and 22 nm while it is about 9 nm for the sol-gel

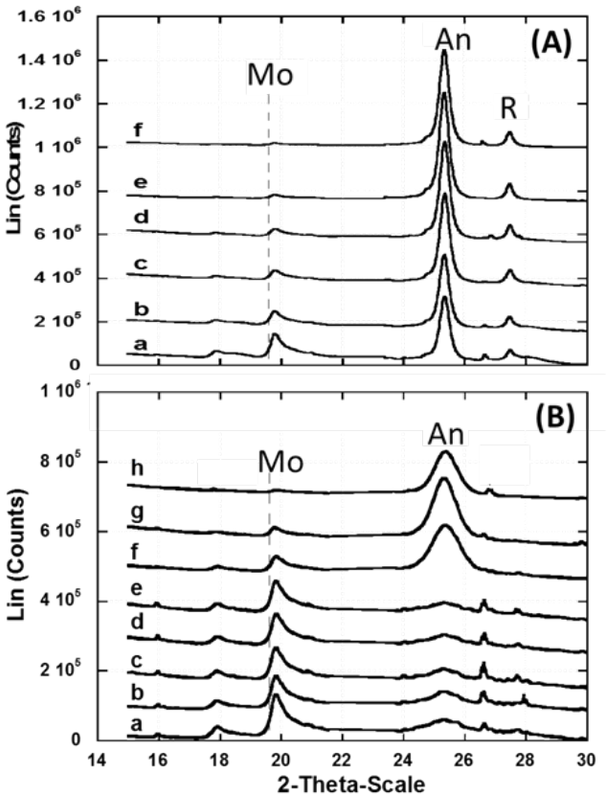

Fig. 1. X-ray diffraction patterns of : (A) P25 TiO_2/bentonite composites prepared with initial masses of titania of: (a) 0.3 g, (b) 0.6 g, (c) 1 g, (d) 1.5 g, (e) 3 g, and (f) 4.5 g. The XRD pattern corresponding to the composite prepared with an initial mass of P25 titania of 2 g is not displayed in the figure for clarity reason. (B) Sol-gel TiO_2/bentonite samples fabricated with initial masses of titanium tetraisopropoxide (IPPT) of: (a) 1 g, (b) 2 g, (c) 3 g, (d) 4 g, (e) 6 g, (f) 8 g, (g) 10 g, and (h) 15.7 g. Parameter: Cu radiation. The symbol "An" corresponds to Anatase while "R" indicates Rutile structure and "Mo" is related to montmorillonite phase.

titania. The sol-gel titania crystallite size is smaller than that of P25. In addition, the layered structure of the bentonite in the composites can be revealed from the XRD patterns. To this aim, it becomes necessary to display the full pattern of the composites, *i.e.* 2θ range from 3°to 64° (Figs. S8 and S10 of the Supporting information). For all the composites, the peak at 2θ = 9° corresponds to the reflection basal peak related to the basal spacing (d_{001} = 9.61). This peak reveals the layered structure of the bentonite in the composites.

The Rietveld analysis is performed within the 2θ range from 15°to 30°. When using P25 titania, it becomes possible to plot the calculated weight percentages of titania deposited onto the bentonite as a function of the initial amounts of TiO_2 in solutions (Fig. 2a). The TiO_2 content increases from 26 to 83 wt.% with the initial mass of P25 catalyst. More interestingly, a linear relationship between the calculated and the initial percentages of titania is reported. The slope of the curve reads as 1.03. This indicates an almost perfect correspondence between the introduced and the immobilized TiO_2 uptakes. In other words, the majority of the catalyst introduced in solution is deposited onto the clay.

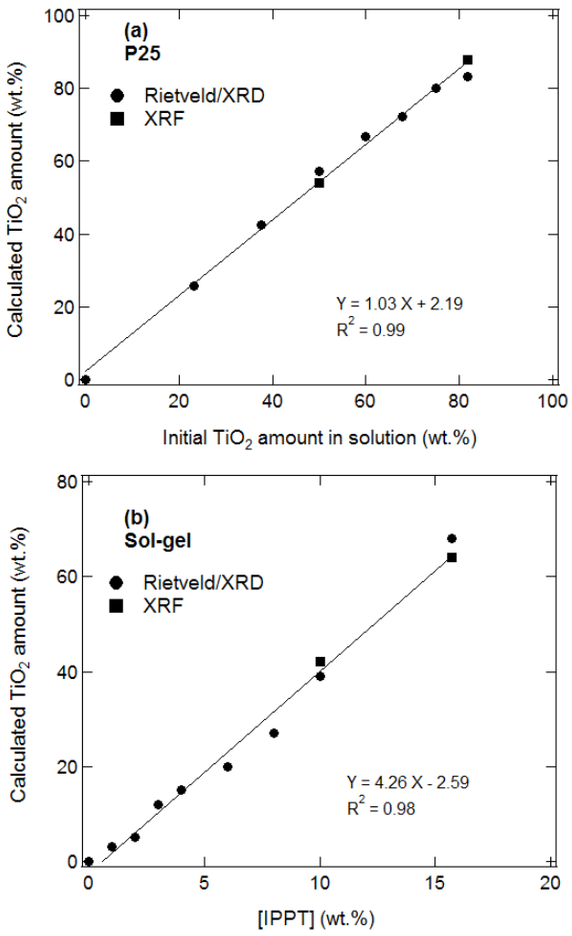

Fig. 2. (a) Comparison between the initial amounts of P25 TiO_2 in solution and the calculated weight percentages of titania incorporated onto the clay. For the estimation of the weight percentage of the initial TiO_2 amount in solution, the mass of titania is relative to the mass of bentonite. (b) Evolution of the calculated weight percentage of sol-gel titania deposited onto the clay with the initial mass of titanium tetraisopropoxide (IPPT) in solution. For the estimation of the weight percentage of IPPT in solution ([IPPT]), the mass of IPPT is normalized by the mass of water. The lines represent the best linear fits. The calculated weight percentages of titania determined by X-ray fluorescence spectroscopy are also shown for comparison (squares, "XRF").

The same analysis is carried out with the composites for which the titania is prepared via the sol-gel process. The calculated weight percentage of titania incorporated onto the clay is plotted against the initial mass of titanium tetraisopropoxide (IPPT) since it is the sol-gel precursor (Fig. 2b). The data indicate a significant titania incorporation into the clay. The TiO_2 uptake increases from 12 to 68 wt.% with the amount of Ti^{4+} present in solution during the synthesis. The weight percentage of titania varies in a linear manner with the IPPT concentration over the entire range of mass of precursor investigated. This linear relationship points out that the IPPT is transformed into TiO_2 and that the titania is deposited onto the bentonite. Note that, under our experimental conditions, a larger amount of P25 TiO_2 (83 wt.%) can be immobilized onto the bentonite compared to that of sol-gel titania (68 wt.%).

The Fig. 2 can be used to compare the calculated weight percentages of titania deposited onto the bentonite determined by the Rietveld approach ("Rietveld/XRD") with those measured by X-ray fluorescence spectroscopy ("XRF"). The overall results of the XRF analysis of the TiO_2/bentonite composites are reported in the Table S1 of the Supporting information S5. For the P25 titania/bentonite materials, the XRF analyses were conducted with initial masses of catalyst in solution of 50 and 82 wt.%. For the sol-gel titania/bentonite composites, the XRF measurements were carried out with initial masses of IPPT of 10 and 17 wt.%. The data from the Rietveld approach and XRF measurements are in good agreement.

3.2. Characterization of the TiO_2/bentonite photocatalysts

Several experiments are performed to characterize the chemical and the surface properties of the composites used for the photo catalysis experiments: TEM, nitrogen adsorption-desorption, and UV/visible spectroscopy measurements.

The TEM images of TiO_2/bentonite composites prepared with P25 and sol-gel titania are displayed in Fig. 3.

Among the TiO_2/bentonite systems, two samples contain approximately the same amount of titanium dioxide, *i.e.* 72 wt.% of P25 titania (Fig. 3a) and 68 wt.% of sol-gel TiO_2 (Fig. 3d). The TEM pictures of the P25 TiO_2/bentonite composite show clearly that the clay particles are packed into the aggregates of TiO_2 (Figs. 3a,b). This result is not surprising considering the large amount of TiO_2 compared to that of the bentonite. The mean size of the individual TiO_2 particles is equal to 20 nm. Conversely, the titanium dioxide particles prepared by the sol-gel method appear uniformly dispersed onto the clay since no aggregate can be detected (Figs. 3c,d). In addition, the TiO_2 powders are integrated into the bentonite structure. The average titania particle diameter is estimated to range between 5 and 10 nm.

The Fig. 4 reports the nitrogen adsorption-desorption isotherms of TiO_2 P25, bentonite, P25 TiO_2/bentonite composite, and bentonite supported sol-gel TiO_2 particles, respectively.

The two composites contain approximately the same TiO_2 content: 72 wt.% of P25 and 68 wt.% of sol-gel. For unsupported TiO_2 P25 (Fig. 4a), it can be observed that both the adsorption and the desorption isotherms have almost no hysteresis loop. In addition, they exhibit a type II isotherm which is associated with non-porous materials. The isotherm corresponding to pure bentonite (Fig. 4b) displays the classical inter particular mesoporosity of smectite characterized by an isotherm of type IV. The surface area is larger for the pure bentonite (S_{BET} (BG) = 75 ± 3 m^2/g) than for the bare titania (S_{BET} (TiO_2) = 57 ± 2 m^2/g). As far as the TiO_2/bentonite systems are concerned, the shape of the isotherms and the surface area are affected by the TiO_2 nature. The isotherm corresponding to the composite prepared with P25 titania (Fig. 4c) seems to be of type II characteristic to non-porous solid. The shape of the isotherm appears similar to that obtained with unsupported P25 TiO_2. The disappearance of the hysteresis previously observed with the raw bentonite may be due to the partial

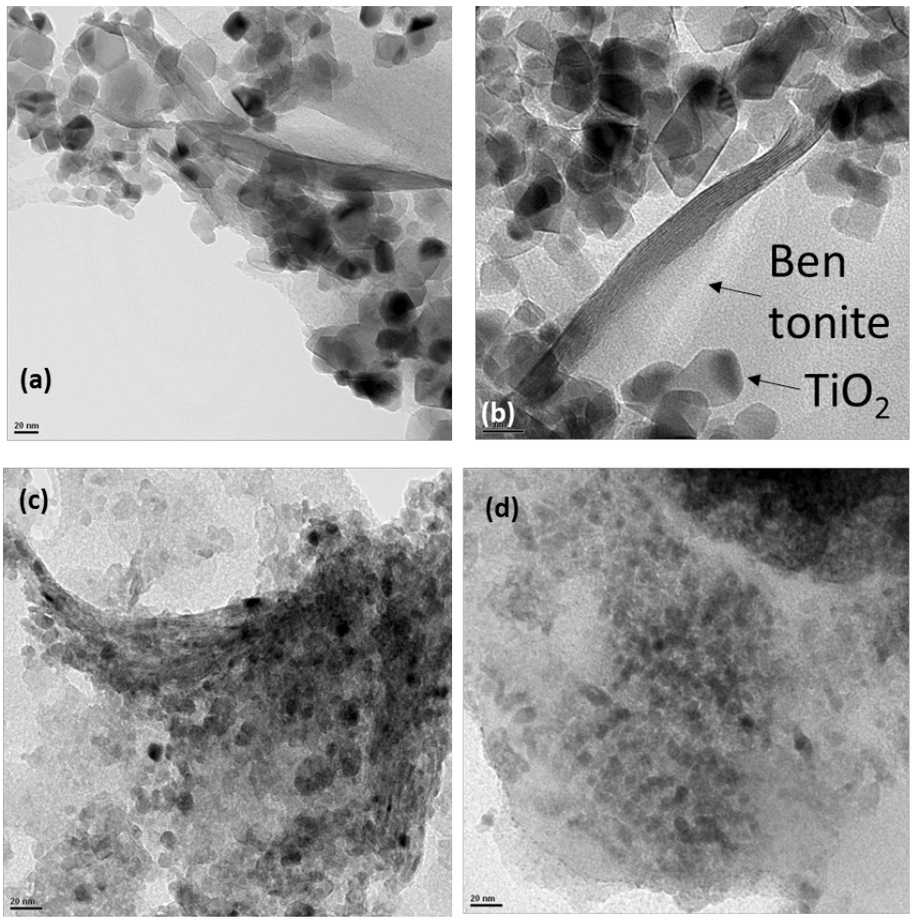

Fig. 3. TEM images of TiO_2/bentonite composites containing: (a) 72 wt.% of P25 titania, (b) 83 wt.% of P25 titania, (c) 39 wt.% of sol-gel titania, and (d) 68 wt.% of sol-gel titania.

destruction of the organization of the clay particles and their dispersion between the aggregates of TiO_2. The lack of hysteresis loop in the adsorption-desorption isotherm confirms the absence of mesoporosity. The BET surface area of the composite reaches S_{BET} (composite) = 73 ± 2 m^2/g regardless of the amount of TiO_2 immobilized. This may suggest the partial exfoliation of the clay particles. In the meantime, it is interesting to note the decrease of microporosity from 7.6 m^2/g, for raw bentonite, to 3.3 m^2/g for the composite. Contrastingly, nitrogen adsorption-desorption measurements of the sol-gel TiO_2/bentonite system (Fig. 4d) display a type IV isotherm that stands for mesoporous materials. A characteristic feature of the Type IV isotherm is its hysteresis loop, which is associated with the capillary condensation taking place into the mesopores. However, the hysteresis appears different than that of pure bentonite. This difference indicates the formation of a specific organization between the clay and the TiO_2 particles. The specific surface area becomes equal to 137 m^2/g. It increases greatly in comparison with those of pure clay (75 m^2/g) and P25 TiO_2/bentonite system (73 m^2/g). This enhancement of the surface area may be related to the exfoliation of the bentonite and/or to the small size of the sol-gel TiO_2 particles. By simple calculation, it can be demonstrated that the surface area S_{BET} (composite) of 137 m^2/g corresponds to the sum of the surface area of the 68 wt.% of TiO_2 and the 32 wt.% of clay (Eq. (1)):

$$S_{BET}(composite) = wt.\%(TiO_2) \times S_{BET}(TiO_2) + wt.\%(BG) \times S_{BET}(BG) \quad (1)$$

where S_{BET} (composite), S_{BET} (TiO_2), and S_{BET} (BG) are the specific surface areas of the composite, the titania particles, and the bentonite, respectively. The notations wt.% (TiO_2) and wt.% (BG) represent the weight fraction of titania and bentonite, respectively. If we consider that the clay conserved its own specific surface area when it is immobilized onto the clay, the remaining surface provided by the TiO_2 particle (S_{BET} (TiO_2)) equals 166 m^2/g. The geometrical calculation of the size of the TiO_2 particles can be obtained using:

$$d_{32}(TiO_2) = \frac{6\varphi}{S_{BET}(TiO_2)} = \frac{6 \times wt.\%(TiO_2)}{S_{BET}(TiO_2) \times \varphi} \quad (2)$$

where the symbol φ reads as the titania volume fraction deposited onto the clay. The geometrical calculation of the size of the sol-gel titania particles using Eq. (2) gives a value of d_{32} (TiO_2) of 6.5 nm, which corresponds well to that estimated by TEM. Based on this result, we suggest that the

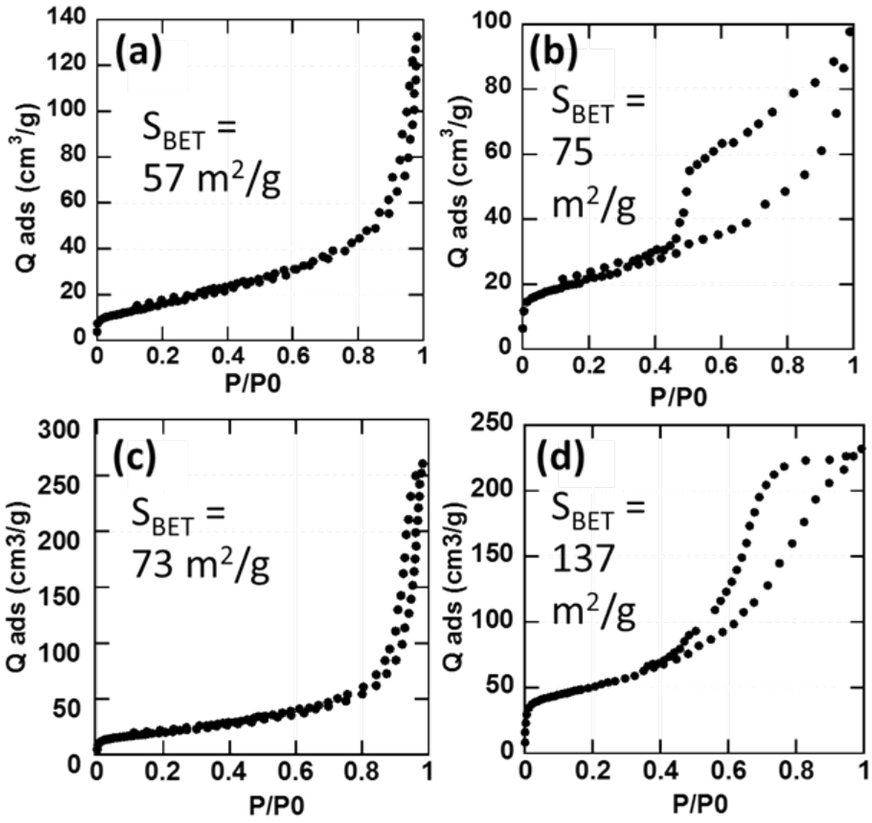

Fig. 4. Adsorption-desorption isotherms of nitrogen on: (a) TiO_2 P25, (b) bentonite, (c) P25 TiO_2/bentonite (72 wt.% of TiO_2), and (d) sol-gel TiO_2/bentonite (68 wt.% of TiO_2). The specific surface areas are indicated in the figure ("S_{BET}").

clay particles are not completely exfoliated, and that the increase in surface area is due the small size of the TiO_2 particles deposited onto the clay.

Diffuse reflectance UV/visible spectroscopy is employed to characterize the optical properties of the TiO_2/bentonite composites. The Fig. 5 represents the influence of the nature and the content of titania on the UV/vis solid absorbance of the bentonites supported TiO_2 particles.

The spectrum of raw bentonite clay (Fig. 5b) presents a regular increase of the absorbance starting at 500 nm up to a maximum at 285 nm. For non-supported P25 titania (Fig. 5a), no absorbance can be detected between 500 and 400 nm. For lower wavelengths, the light absorption increases with the diminution of the wavelength and then reaches a pseudo-plateau at 300 nm. The optical absorption of titanium dioxide for wave lengths shorter than 400 nm is generally explained by the charge-transfer from O^{2-} to Ti^{4+}, related to electron excitation from the valence band to the conduction band [39]. More interestingly, the absorbance curves for raw P25 titania and TiO_2/bentonite composites display the same shape regardless of the titania nature and loading. The similarity in the spectra shapes emphasizes that the absorption of the light occurs preferentially with the titania particles for the TiO_2/bentonite systems. This may be attributed to (i) the large amount of titania compared to that of the clay and/or (ii) to the fact that the clay particles are packed in the TiO_2 aggregates. Logically, the optical behavior can be related to the titania content. As the TiO_2 amount deposited onto the clay is enhanced, the absorbance curve shifts to higher amplitudes. In other words, the absorbance value at the plateau (wavelengths lower than or equal to 300 nm) increases regularly with the titania content. The nature of the titania particles affects also the absorbance values. The light absorptions of the composites prepared with sol-gel titania are markedly improved compared to those obtained with P25 titanium dioxide. On the one hand, the absorbance remains larger for the sample containing 68 wt.% of sol-gel TiO_2 compared to that with 72 wt.% of P25 TiO_2. On the other hand, the spectra of raw TiO_2 P25 (100 wt.%) and bentonite containing 68 wt.% of sol-gel titania have approximately the same absorbance values since the two curves collapse. Our result corroborates the other studies, demonstrating that the efficiency of UV light absorption is elevated by the reduction of the titania particle size [40].

The direct band gap energy of the composites (E_g) can be extracted from the UV/visible data by using the Kubelka-Munk relationship:

$$(\alpha h\upsilon)^2 = A\,(h\upsilon - E_g) \tag{3}$$

where $h\upsilon$ denotes the photon energy, α refers to the absorption coefficient, and $\underline{A}$ is a constant. The value of E_g is

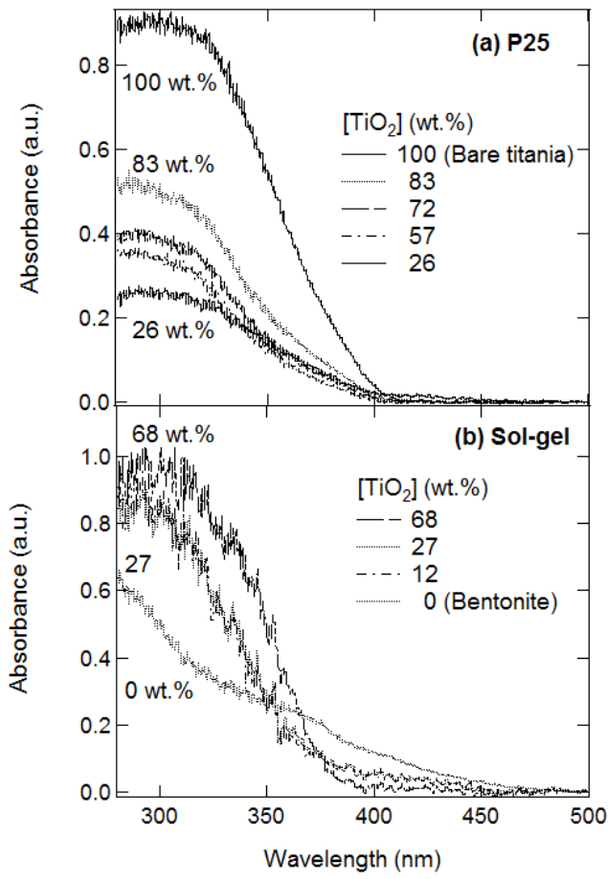

Fig. 5. UV/visible diffuse reflectance spectra of TiO_2/bentonite composites.

obtained from a plot of $(\alpha h\nu)^2$ versus photon energy ($h\nu$). The intercept of the tangent of the plot gives the value of E_g (Fig. S12 of the Supporting information S6). The band gap energies are reported in the Table 1. The band gap slightly increases, from 3.37 eV to 3.49 eV, with the diminution of the titania content regardless of the TiO_2 nature. In addition, the band gap values are equivalent for the composites prepared with sol-gel and P25 titania.

3.3. Photocatalytic capacity of TiO_2 immobilized onto bentonite

It has been widely described in the literature that the pH of the solutions has a strong impact on both the adsorption and the photo degradation of organic compounds and dyes [5,7,41]. All the former studies illustrated that the variation of the pH induces major changes in the charge density of the surface and the molecules. For this reason, the adsorption capacity and the photo catalytic activity of the composites are investigated separately at pH 10 and 3.

3.3.1. Basic pH

The effect of the titania nature and content immobilized onto the bentonite on the kinetics of the photo catalytic degradation of methyl orange at pH 10 is illustrated in Fig. 6. The data at irradiation time 0 correspond to the remaining pollutant concentration after one hour of stirring in the dark. Consequently, they give access to the adsorption capability of the samples.

A weak adsorption of methyl orange on raw bentonite and bentonite supported TiO_2 is reported since there is a very slight diminution of the methyl orange concentration after 60 min of dark period (Fig. 6 and Fig. S11 of the Supporting

Table 1
Band gap versus the amount and the nature of TiO_2 deposited onto the bentonite

TiO_2 content (wt.%), nature	Band gap E_g(eV)
100%, P25	3.37
83%, P25	3.48
72%, P25	3.47
57%, P25	3.49
26%, P25	3.48
68%, Sol-gel	3.42
27%, Sol-gel	3.46
12%, Sol-gel	3.46

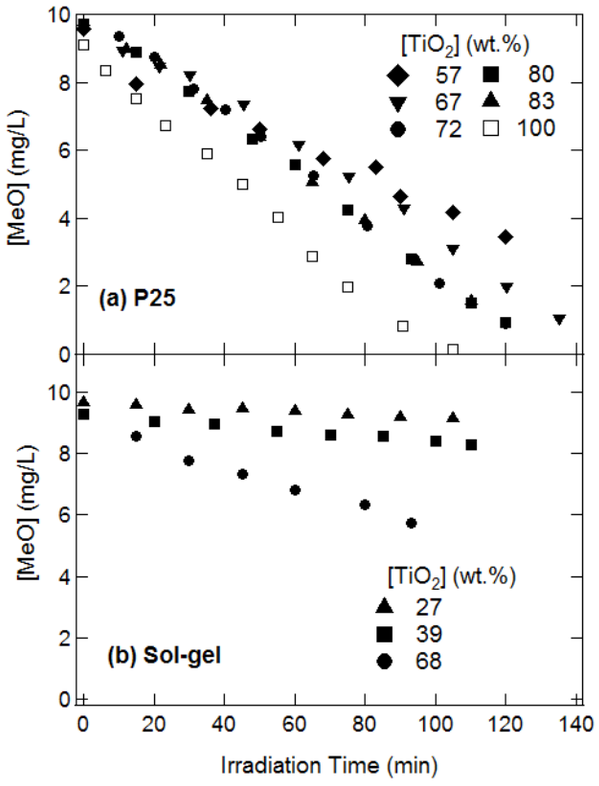

Fig. 6. Photo catalytic degradation of methyl orange (MeO) at pH 10 as a function of the time of irradiation for the TiO_2/bentonite composites prepared with (a) P25 and (b) sol-gel titania. The unsupported P25 titania without bentonite is shown for comparison ([TiO_2] = 100 wt.%, empty square symbol).

information S4). In addition, the pollutant uptake does not substantially change with the titania loading. At basic pH, the bentonite and the titania are negatively charged (zeta potentials of ca. –40 mV, see Fig. S1 of the Supporting information) while the acidity constant of methyl orange is equal to 3.75. The small value of the pollutant adsorbed amounts can be explained by the electrostatic repulsions between the pollutant and the catalyst.

As far as the photocatalytic activity of the raw bentonite is concerned, the UV exposure period shows no diminution of the methyl orange concentration with the irradiation time (Fig. S11 of the Supporting information S4). This validates the lack of photocatalytic efficiency for bentonite clay in the degradation of methyl orange. Conversely, all the TiO_2/bentonite composites have a photocatalytic activity because they produce the degradation of the contaminant dissolved in water (Fig. 6). However, the photocatalytic performances are significantly affected by both the type and the amount of titania deposited onto the clay. On the one hand, methyl orange photo degradation proceeds more favorably with the composites prepared with P25 TiO_2 (Fig. 6a) than with sol-gel titanium dioxide (Fig. 6b).The difference in the photocatalytic activity cannot be related to the variation of the surface area because the pollutant adsorbed amounts remain very low and roughly similar for all the composites. As a matter of fact, the photochemical properties can be used to explain the photocatalytic results. In general, photo catalysts displaying large UV light absorption are expected to exhibit enhanced photocatalytic activity if the photonic efficiencies do not differ substantially. However, sol-gel TiO_2 immobilized onto bentonite have greater UV light absorption than those of P25 TiO_2/bentonite composites but they lead to weaker degradation. This points out that the photo chemical activity seems to be mainly driven by the nature and the proportion of the crystallographic phases of the titania. This phenomenon has been widely described in the literature [6,26,27]. It seems now well established that the titania nanoparticles with mixed crystallographic phases, such as P25 (15 % rutile and 85 % anatase), have better photocatalytic activity than pure anatase TiO_2. The greater photocatalytic properties of the mixed phase P25 TiO_2 results from the photoexcited charge migration between the anatase and the rutile phases which produces a synergetic effect in the charge separation [26]. However, the present case is more complicated since the amount of amorphous phase of TiO_2 and the packing of the titania onto the clay can also influence the photo degradation performances. The proportion of amorphous phase is larger for TiO_2 prepared via the sol-gel method in comparison to that of P25 titania (Figs. S4 and S6 of the Supporting information). The amorphous phase contained to some extent in the materials prepared by sol-gel has been reported to play a negative effect on the photocatalytic activity. The amorphous phase, which usually comprises numerous defects, *i.e.* impurities, dangling bonds, and microvoids, behaves as recombination centers for the photo induced electron/hole (e^-/h^+) pairs. Concerning the packing of the titania onto the clay, we previously reported that the clay particles are packed into the aggregates of TiO_2 for P25/TiO_2 composites (Figs. 3a,b). Conversely, the titanium dioxide particles prepared by the sol-gel method appear uniformly dispersed onto the clay (Figs. 3c,d).The better degradation efficiency reported with P25/bentonite systems can be also explained in terms of the availability of the titania active sites of titania on the clay surface. The total active surface area is larger with P25 than with sol-gel. The term active includes the area exposed to radiation which appears different than the BET surface area. The low active surface area of the sol-gel TiO_2/composites might be due to the fact that a part of the titania is incorporated into the mesopores of the clay where the radiation does not reach. Consequently, they cannot be activated by the radiation and are not "active".

Concerning the titania concentration, it appears that the reduction of the titania loading extends the duration of degradation. The highest methyl orange degradation takes place with the unsupported P25 titanium dioxide which represents the largest TiO_2 content, *i.e.* 100 wt.% of titania. The degradation occurs after 105 min of irradiation. It is interesting to investigate the oxidation products formed during the reaction. Table 2 reports the TOC of the solutions at the end of the process (irradiation time = 120–130 min). For the P25 titania/bentonite composites containing a TiO_2 content larger than or equal to 67 wt.%, the TOC values range between 1.5 and 2.6 mg carbon/L. This seems to confirm the total degradation of the dye and also the absence of byproducts. However, for the composite containing a P25 TiO_2 content of 57 wt.%, and the sol-gel titania/bentonite systems, the TOC remain at a high level (5.7–15.2 mg carbon/L). The methyl orange could not be completely mineralized after 2 h of reaction under UV light.

It appears relevant to study in details the kinetics of the reactions. For all the photocatalysts, the pollutant concentration decreases linearly with the irradiation time. This attests that the reaction rate (r) follows a zero-order kinetic ($r = k$). Consequently, the values of the rate constant (k) can be estimated from the slope of the straight line in the plot of the contaminant concentration as a function of the irradiation time. Fig. 7 presents the evolution of the rate constant as a function of the titania loading deposited onto the bentonite for P25 and sol-gel titanium dioxides.

The rate constant increases as the titania content incorporated in the composite is extended. The addition of higher quantities of TiO_2 photocatalyst onto the clay improves the total active surface area and the amount of generated

Table 2
Photocatalytic degradation of methyl orange at pH 10 for the P25 and sol-gel TiO_2/bentonite composites. Total organic carbon ("TOC solution") of the final solutions at the end of the process

TiO_2 content (wt.%), nature	TOC solution (mg carbon/L)
100%, P25	1.6
83%, P25	2.6
80%, P25	1.5
72%, P25	1.5
67%, P25	1.7
57%, P25	5.7
68%, Sol-gel	9.5
39%, Sol-gel	13.8
27%, Sol-gel	15.2

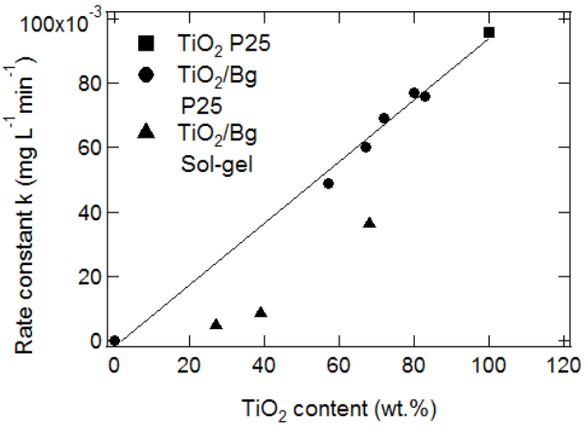

Fig. 7. Reaction rate constant (k) at pH 10 versus the amount of TiO_2 deposited onto the bentonite ([TiO_2]). The line represents the best linear fit given by k = 0.001 [TiO_2 P25] – 0.0017 (R^2 = 0.993). The value of the reaction rate constant obtained with TiO_2 P25 without bentonite is shown for comparison (square, "TiO_2 P25").

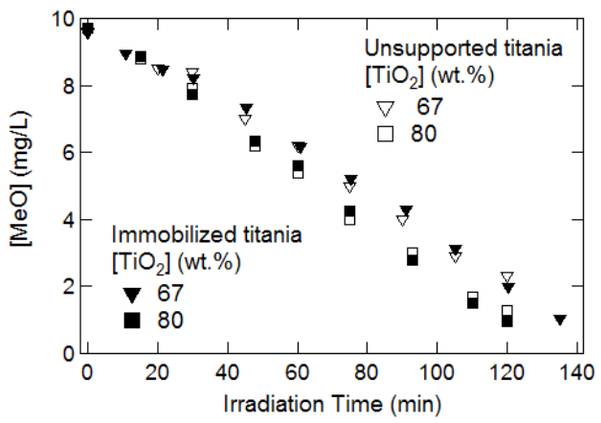

Fig. 8. Comparison of the change in the methyl orange concentration ([MeO]) as a function of the time of irradiation at pH 10 for unsupported P25 titania and TiO_2 P25 immobilized onto bentonite.

hydroxyl radicals. Recall that these radicals produce the photocatalytic oxidation reactions [1–5]. On the one hand, the values of the constant k depend strongly on the type of titania catalyst. At the same titania content, the kinetic constant, *i.e.* the amount of hydroxyl radicals formed, with sol-gel titania catalyst remains always lower than that obtained with P25 catalyst. For instance, for composites containing 68 wt.% of titania, the rate constant is around 0.036 mg L^{-1} min^{-1} for sol-gel titania while k = 0.060 mg L^{-1} min^{-1} for P25 catalyst. On the other hand, the constants behave differently depending on the nature of the catalyst. For sol-gel titania, there is a non-linear increase of the rate constant with the catalyst surface coverage. Conversely, the kinetic constant depends linearly on the P25 TiO_2 content and can be represented by the straight line in Fig. 7. This result establishes that the quantity of titania deposited onto the bentonite is the dominant factor that controls the capacity of the composites towards the decomposition of the pollutant. This confirms that the photodegradation of the dye occurs only at the surface of the TiO_2 catalyst since the increase in the titania loading leads to an enhancement of the degradation rate of the dye. Although, this linear behaviour has been expected, it has been barely reported in the scientific literature. To the best of our knowledge, only one study relates a pseudo-linear increase of the rate constants of acid orange 7 degradation with the deposited titania concentrations for TiO_2/Mg_2FeCO_3 synthetic layer double hydroxide composites [42]. Note also that the constant obtained with the unsupported titania (100 wt.% P25) falls on this single line. This illustrates that the photocatalytic properties of the P25 titania are not altered when deposited onto the bentonite. Similar phenomenon has been described in the case of TiO_2 pillared montmorillonite [19]. In order to confirm this result, it seems interesting to directly compare the time evolution of the methyl orange concentration during the photocatalytic reaction, using the same P25 titania content, for unsupported titania and TiO_2 immobilized onto the bentonite (Fig. 8). At all the photocatalyst concentrations, unsupported and immobilized TiO_2 behave similarly. No significant difference is observed in terms of adsorbed amount and photocatalytic performance. This confirms that, at basic pH, the bentonite plays no role in the degradation activity and that the bentonite does not modify the photocatalytic properties of the P25 titanium dioxide. This seems to establish that the titania in the TiO_2/bentonite systems and the non-immobilized titania display similar state of aggregation of the photocatalysts onto the clay and in the solution. Under these conditions, the same amount of catalyst particles could be optically activated in solution and onto the clay.

3.3.2. Acidic pH

It becomes interesting to investigate the behavior of the composites at acidic pH. First, the P25 TiO_2 particles are adopted for the exploration of the adsorption and the photocatalytic degradation of methyl orange at pH 3 in the presence of bentonite containing various amounts of titania (Fig. 9a).

The dye adsorbed amount becomes much higher on the raw bentonite (9.6 mg/g) than onto the unsupported titania (1.1 mg/g). These uptake values appear compatible with those reported from the literature [6,7,43]. For bare positively charged TiO_2, there is no specific interaction with the uncharged pollutant. Oppositely, the higher amount of methyl orange adsorbed onto the bentonite is generally attributed to hydrogen bonding interactions between the dye species and the clay surface [43]. For the TiO_2/bentonite composites, the adsorption capacity remains large and is affected by the titania surface coverage onto the clay. In the presence of the photocatalyst onto the clay surface, the pollutant uptake remains lower than that obtained with the raw bentonite and it gradually decreases with the TiO_2 content. Consequently, the immobilization of titania onto the bentonite diminishes the adsorption capability of the bentonite for the dye. Considering that the methyl orange adsorption occurs preferentially onto the clay, the adsorption trend can

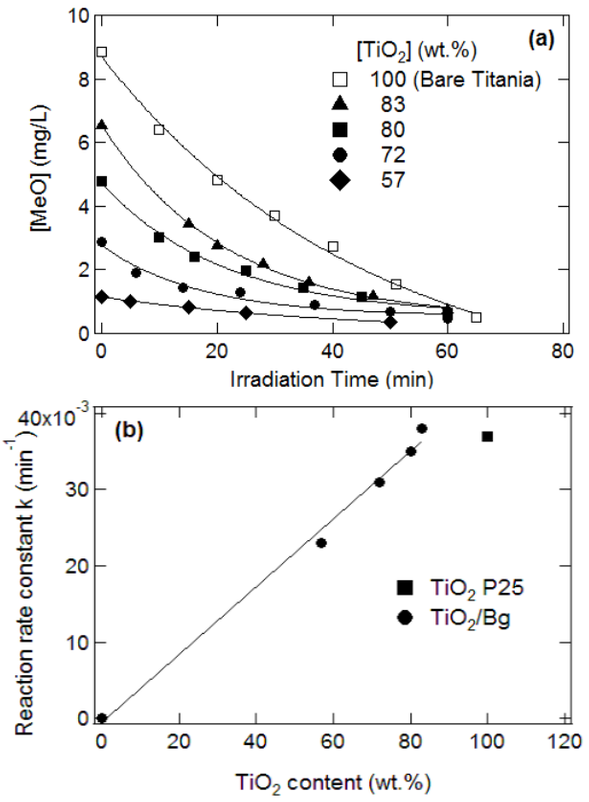

Fig. 9. (a) Photocatalytic degradation of methyl orange (MeO) at pH 3 as a function of the time of irradiation for the unsupported P25 titania and P25 TiO_2/bentonite composites. The lines correspond to the fit of the experimental data by a first order exponential decay function of the form A exp (–k × t) consistent with a first order kinetics. (b) Reaction rate constant (k) versus the amount of TiO_2 deposited onto the bentonite ([TiO_2]). The line represents the best linear fit given by k = 0.0004 [TiO_2] – 0.0006 (R^2 = 0.993). The value of the reaction rate constant obtained with TiO_2 without bentonite is shown for comparison (square, "TiO_2 P25").

be explained by the fact that the methyl orange adsorption and the TiO_2 immobilization occur onto the same surface sites of the clay. In other words, the titania particles are immobilized onto the bentonite prior to contact with the contaminant which, then, hinders the pollutant adsorption onto these bentonite adsorption sites.

Under UV light irradiation, the complete methyl orange degradation is achieved with all the samples. TOC analysis is employed to support this interpretation. The TOC values of the solutions at the end of the process (irradiation time = 60–80 min) range between 1.2 and 2.4 mg carbon/L (Table 3, "TOC solution"). This seems to confirm the total degradation of the dye and also the absence of byproducts. However, we are aware that a high percentage of methyl orange could remain adsorbed onto the material without being degraded. The absence of methyl orange molecules onto the catalyst at the end of the photocatalytic process was evaluated by measuring the amount of TOC in the liquid after washing. The physisorbed pollutant molecules can be removed by contact with solvent for several hours at

Table 3
Photocatalytic degradation of methyl orange at pH 3 for the unsupported P25 titania and P25 TiO_2/bentonite composites. Total organic carbon of the final solutions at the end of the process ("TOC solution") andin the liquids after washing("TOC rinsing")

TiO_2 content (wt.%)	TOC solution (mg carbon/L)	TOC rinsing (mg carbon/L)
100%	1.2	0.7
83%	2.4	1.8
80%	1.7	1.2
72%	2.2	1.8
57%	1.8	1.0

room temperature. We used the following washing procedure: washing with pure water during 3 hours. At the end of the rinsing step, the particles were centrifuged. The possible presence of methyl orange molecules in the supernatant (desorbed) was measured by organic carbon titration. For all the samples, the Table 3 indicates that a very small amount of carbon remains in the suspension ([TOC rinsing] = 0.7–1.8 mg carbon/L). This carbon content is very close to the mean value of TOC measured on our "pure" water. These results imply that no methyl orange molecules and byproducts are desorbed during the washing. We then consider the total degradation of the dye, and also the absence of byproducts regardless of the titania content.

However, the immobilization of the titania onto the clay reduces the time of degradation. This may appear surprising because it corresponds to a relatively weak titania uptake deposited onto the surface of the clay (57–83 wt.%) compared to that of the unsupported titania (100 wt.%). It can then be deduced that the pollutant adsorbed amount has a strong impact on the time necessary to totally degrade the pollutant. In details, the reaction time shortens with the pollutant surface coverage. Similar relationship between the time to degrade the pollutant and the contaminant adsorbed amount was previously demonstrated for different catalysts and target pollutants [41,44,45]. The lowest time of degradation is obtained with the composite containing the smallest amount of photocatalyst (57 wt.% of titania) but with the largest uptake of pollutant adsorbed. In other words, with a decrease of the titania loading, the capability of photodegradation of the dye increases because the large contaminant surface concentration provides more molecules to react with the radicals.

The variation of the methyl orange concentration (C) with respect to the irradiation time (t) corresponds to an exponential shape which is characteristic of a first-order kinetic reaction ($C = C_0 \exp(-k \times t)$) regardless of the titania loading. Note that C_0 stands for the initial pollutant concentration in the bulk solution after the dark adsorption (at irradiation time = 0).The reaction rate constant k can be utilized to discuss the relation between the titania content deposited onto the bentonite and the photochemical performance, *i.e.* the formation of radicals. The Fig. 9b illustrates the effect of the TiO_2 content on the values of the photocatalytic rate constant. There is a significant correlation between the rate of degradation and the titania amount immobilized onto the

clay since k increases linearly with the photocatalyst loading. This confirms that the TiO_2 photocatalyst plays a dominant role on the photochemical activity and the radical formation. Another interesting feature is that the kinetic constant of the unsupported TiO_2 (without bentonite) is not included in the linear evolution. It seems evident that the composite containing 83 wt.% of titania displays the same photochemical activity than that of the raw TiO_2 in the absence of bentonite (100 wt. % of titanium dioxide) while the amounts of photocatalyst remain different. The unsupported TiO_2 contains 1 g of catalyst while the composite consists of 0.83 g of titania. Based on the experimental equation of the curve obtained with the composites, a kinetic constant k of 0.0437 min^{-1} may be extrapolated with 100 wt.% of deposited TiO_2 instead of the experimental value of 0.0370 min^{-1} reported with raw titania. This phenomenon was already described in the literature. One example was given by Zhang et al. [46] for the photocatalytic decomposition of water with CdS/bentonite nanocomposites. The greater photochemical activity of the TiO_2/bentonite systems compared to that of the non-immobilized titania is probably attributed to the different state of aggregation of the photocatalysts onto the clay and in the solution. The nanoparticles seem to produce larger aggregates in solution compared to those obtained onto the clay. Under these conditions, less catalyst particles could be optically activated in solution.

It seems also interesting to discuss the effect of the structural properties of the composite on the photocatalytic activity by comparing the time evolution of the methyl orange concentration during the photooxidation reaction, under similar experimental conditions, for the composite and a simple mixture of TiO_2 P25 and bentonite (Fig. 10). The mixture was prepared, just before the photocatalysis experiments, by mixing an aqueous suspension of titania with an aqueous dispersion of bentonite under stirring. The methyl orange adsorbed amount appears larger onto the mixture than onto the composite. However, the dye photodegradation proceeds more favorably with organized titania/bentonite composite than in the presence of non-attached mixture of TiO_2 and bentonite. This result confirms that the titania organization and immobilization onto the clay could be the main cause of the large activity during the photooxidation process.

The same experiments were conducted with the composites for which the titania was synthesized by the sol-gel method (results not shown). On the one hand, the samples have also a strong methyl orange adsorption. The dye concentrations after 60 min of dark period amount to 2.6, 1.1 and 0.8 mg/L, for the composites containing 68 wt.%, 39 wt.% and 27 wt.% of sol-gel titania. The dye uptake seems unaffected by the nature of the titania since the adsorbed amounts are equivalent for the samples containing 68 wt.% of sol-gel TiO_2 and 72 wt.% of P25 TiO_2. As previously observed with P25 titania, the contaminant surface coverages onto the composites remain lower than that obtained with the raw bentonite. In addition, the methyl orange uptake gradually decreases with the titania loading immobilized onto the clay. On the other hand, since the methyl orange photodegradation by the sol-gel titania/bentonite systems is weak, it was not possible to precisely evaluate the times of complete degradation of the pollutant.

We have previously demonstrated that the photodegradation performance of the composites is related to the

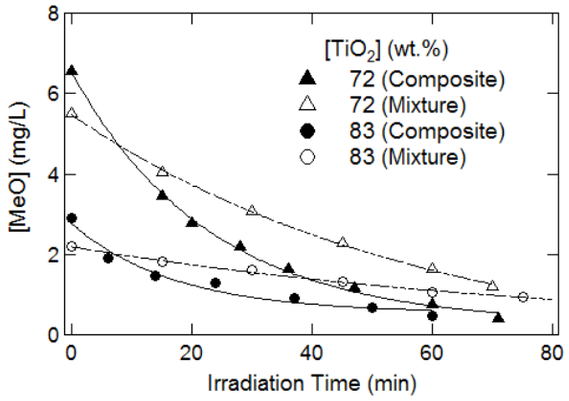

Fig. 10. Comparison of the change in the methyl orange concentration ([MeO]) as a function of the time of irradiation at pH 3 for TiO_2 P25 immobilized onto bentonite ("Composite") and a simple mixture of titania P25 and bentonite ("Mixture"). The lines correspond to the fit of the experimental data by a first order exponential decay function of the form A exp ($-k \times t$) consistent with a first order kinetics.

adsorption capacity of the clay. However, only one dye (methyl orange) was used as target pollutant. It seems interesting to discuss whether similar results can be obtained using other organic contaminants. Thus, the photocatalytic decomposition of salicylic acid, at pH 3, using various contents of P25 titania immobilized onto the bentonite is reported in the Fig. 11a.

As previously observed with methyl orange, the composite adsorption capability depends on the titania surface coverage. The salicylic acid adsorbed amount increases with the reduction of the TiO_2 content. The salicylic acid uptakes are lower than those obtained with methyl orange. This result is not surprising since the adsorption capacity of the bentonite towards methyl orange appears larger than that for salicylic acid [47]. The complete photodegradation of salicylic acid takes place with all the composites. The TOC data at the end of the process are comprised between 1.1 and 2.5 mg carbon/L regardless of the titania loading (Table 4, "TOC solution"). In addition, the absence of salicylic acid molecules onto the composites at the end of the photocatalytic process was evaluated by measuring the amount of TOC in the liquids after washing. For all the samples, the Table 4 indicates that a very small amount of carbon remains in the suspension ([TOC rinsing] = 1.1–1.8 mg carbon/L). These results demonstrate that no salicylic acid molecules and byproducts are desorbed during the washing. This establishes the total degradation of the pollutant. Similarly to that reported with the dye, the time required for the complete photodegradation of salicylic acid is correlated to the adsorption capacity of the clay. The salicylic acid degradation takes place earlier on the bentonite-supported samples than on the pure titania. More precisely, the reaction time decreases with the increase of the salicylic acid adsorbed amount. In addition, the linear relationship between the obtained rate constants k and the P25 titania surface coverages (Fig. 11b) corresponds perfectly to the trend already reported with methyl orange. Again, it appears that the kinetic constant of the unsupported TiO_2

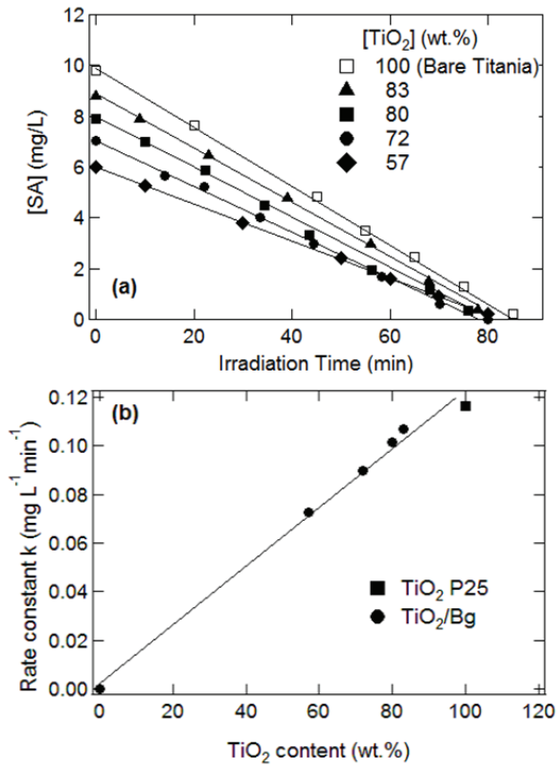

Fig. 11. (a) Photocatalytic degradation of salicylic acid (SA) at pH 3 as a function of the time of irradiation for the unsupported P25 titania and P25 TiO_2/bentonite composites. The lines correspond to the linear fit of the experimental data. (b) Reaction rate constant (k) versus the amount of TiO_2 deposited onto the bentonite ([TiO_2]). The line represents the best linear fit given by $k = 0.0013\ [TiO_2] - 0.0002$ ($R^2 = 0.994$). The value of the reaction rate constant obtained with TiO_2 without bentonite is shown for comparison (square, "TiO_2 P25").

Table 4
Photocatalytic degradation of salicylic acid at pH 3 for the unsupported P25 titania and P25 TiO_2/bentonite composites. Total organic carbon of the final solutions at the end of the process ("TOC solution") and in the liquids after washing ("TOC rinsing")

TiO_2 content (wt.%)	TOC solution (mg carbon/L)	TOC rinsing (mg carbon/L)
100%	1.1	1.8
83%	2.5	1.1
80%	1.8	1.3
72%	2.4	1.7
57%	1.2	1.5

is not included in the linear evolution and is slightly lower than the value extrapolated from the straight line.

To summarize, our data point out that the time necessary to totally degrade the pollutants shortens with the diminution of the titania loading. At the same time, the kinetic constant is reduced while the contaminant adsorbed amount is increased. The faster degradation is attributed to the larger adsorption of the pollutants onto the bentonite sites which compensates the small amount of titania photodegradation sites and the low uptake of radicals.

4. Conclusions

In this paper, we evaluate the impact of the TiO_2 nature and content immobilized onto bentonite on the adsorption capacity and the photocatalytic removal of methyl orange and salicylic acid from water towards TiO_2/bentonite composites at pH 3 and 10. Two methods were applied to prepare the bentonite supported titania particles. The first route employed commercial titania P25 as photocatalyst. The positively charged TiO_2 particles were coagulated with the negatively charged clay layers. For the other preparation method, the titania was synthetized by the sol-gel technique. The titanium sol solution was mixed with the clay aqueous suspension to immobilize the TiO_2 onto the clay. The composites are characterized by means of TEM, XRD, nitrogen adsorption-desorption, and UV/visible spectroscopy measurements. A Rietveld-based fitting method of X-ray powder diffraction patterns has been employed to determinate quantitatively the TiO_2 content deposited onto the clay. A significant amount of TiO_2 is incorporated onto the clay: from 57 to 83 wt.% of P25 and from 27 to 68 wt.% of sol-gel.

The structural properties of the composite appears as one of the key parameter which affects the process efficiency. The pollutant photooxidation proceeds more favorably with organized titania/bentonite composite than in the presence of non-attached mixture of TiO_2 and bentonite. The packing of the titania onto the clay affects the availability of the active sites of titania for the pollutant and the light. A better photoactivity is obtained when the clay particles are embedded into the aggregates of TiO_2 than when the titania is uniformly dispersed onto the surface and the mesopores of the clay.

As far as the photochemical properties of the composites are concerned, greater photodegradation of the dye occurs with bentonites impregnated with mixed crystallographic phases P25 TiO_2 (15 % rutile and 85 % anatase) than with pure anatase sol-gel titanium dioxide. The higher photochemical activity results from the photoexcited charge migration between the anatase and the rutile phases which produces a synergetic effect in the charge separation. In addition, a linear relationship between the reaction rate constant of degradation and the titania loading immobilized onto the clay is revealed. This indicates that the TiO_2 particles play the dominant role on the photochemical activity and the formation of the hydroxyl radicals.

The photodegradation performances of the composites can be related to the adsorption capacity of the clay which is pH-dependent. When the adsorption of the pollutant remains low (at basic pH), the bentonite plays no role in the degradation efficiency. At the same TiO_2 content, the photocatalytic activities of the unsupported and immobilized titania are equivalent. On the opposite, at pH 3 the pollutant adsorption becomes significant. The contaminant adsorbed amounts onto the composites remain lower than that obtained with the raw bentonite. In addition, the pol-

lutant uptake gradually decreases with the titania loading immobilized onto the clay. This emphasizes that the pollutant adsorption and the TiO_2 particles immobilization occur onto the same surface site of the clay. All the composites produce the complete degradation of the contaminants. The immobilization of the titania leads to a reduction of the time necessary to totally degrade the pollutants compared to that of the unsupported TiO_2. The fastest photocatalytic degradation is reached with the composite containing the lowest amount of titania (57 wt.%) but with the largest uptake of pollutant adsorbed. This confirms that the contaminant adsorption onto the composite is an essential parameter for the efficient decomposition of the pollutants despite the reduction of the photodegradation sites and the relatively low amount of radicals.

References

[1] M.R. Hoffmann, S.T. Martin, W. Choi, D.W. Bahnemann, Environmental applications of semiconductor photocatalysis, Chem. Rev., 95 (1995) 69–96.

[2] J.M. Herrmann, Photocatalysis fundamentals revisited to avoid several misconceptions, Appl. Catal. B: Environ., 99 (2010) 461–468.

[3] T. Ahmed, S. Imdad, K. Yaldram, N.M. Butt, A. Pervez, Emerging nanotechnology-based methods for water purification: a review, Desal. Water Treat., 52 (2014) 4089–4101.

[4] A. Fujishima, T.N. Rao, D.A. Tryk, Titanium dioxide photocatalysis, J. Photochem. Photobiol. C: Photochem. Rev., 1 (2000) 1–21.

[5] U.I. Gaya, A.H. Abdullah, Heterogeneous photocatalytic degradation of organic contaminants over titanium dioxide: a review of fundamentals, progress and problems, J. Photochem. Photobiol. C: Photochem. Rev., 9 (2008) 1–12.

[6] K. Zimny, T. Roques-Carmes, C. Carteret, M.J. Stébé, J.L. Blin, Synthesis and photoactivity of ordered mesoporous titania with a semicrystalline framework, J. Phys. Chem. C, 116 (2012) 6585–6594.

[7] J.L. Blin, M.J. Stébé, T. Roques-Carmes, Use of ordered mesoporous titania with semi-crystalline framework as photocatalyst, Colloids Surf. A, 407 (2012) 177–185.

[8] S. Pazokifard, S.M. Mirabedini, M. Esfandeh, M. Mohseni, Z. Ranjbar, Silane grafting of TiO_2 nanoparticles: dispersibility and photoactivity in aqueous solutions, Surf. Interface Anal., 44 (2012) 41–47.

[9] C. Wang, H. Mao, C. Wang, S. Fu, Dispersibility and hydrophobicity analysis of titanium dioxide nanoparticles grafted with silane coupling agent, Ind. Eng. Chem. Res., 50 (2011) 11930–11934.

[10] O. Carp, C.L. Huisman, A. Reller, Photoinduced reactivity of titanium dioxide, Prog. Solid State Chem., 32 (2004) 33–177.

[11] M.F.J. Dijkstra, H.J. Panneman, J.G.M. Winkelman, J.J. Kelly, A.A.C.M. Beenackers, Modeling the photocatalytic degradation of formic acid in a reactor with immobilized catalyst, Chem. Eng. Sci., 57 (2002) 4895–4907.

[12] R.R. Sheha, A.H. Harb, I.E.T. El-sayed, H.H. Someda, Removal of ethylenediaminetetraacetic acid and its cobalt complex by layered double hydroxide/titanium dioxide from aqueous solution, Desal. Water Treat., 57 (2016) 16466–16472.

[13] M.N. Chong, B. Jin, C.W. Chow, C. Saint, Recent developments in photocatalytic water treatment technology: A review, Water Res., 44 (2010) 2997–3027.

[14] E. Rossetto, D.I. Petkowicz, J.H.Z. dos Santos, S.B.C. Pergher, F.G. Penha, Bentonites impregnated with TiO_2 for photodegradation of methylene blue, Appl. Clay Sci., 48 (2010) 602–606.

[15] Z. Sun, Y. Chen, Q. Ke, Y. Yang, J. Yuan, Photocatalytic degradation of a cationic azo dye by TiO_2/bentonite nanocomposite, J. Photochem. Photobiol. A: Chem., 149 (2002) 169–174.

[16] F.F. Cai, Z.H. Yang, J. Huang, G.M. Zeng, L.K. Wang, J. Yang, Application of cetyltrimethylammonium bromide bentonite–titanium dioxide photocatalysis technology for pretreatment of aging leachate, J. Hazard. Mater., 275 (2014) 63–71.

[17] Z.M. Xie Chen, Y.Z. Dai, Preparation of TiO_2/sepiolite photocatalyst and its application to printing and dyeing wastewater treatment, Environ. Sci. Technol., 32 (2009) 123–127.

[18] D. Karamanis, A.N. Okte, E. Vardoulakis, T. Vaimakis, Water vapor adsorption and photocatalytic pollutant degradation with TiO_2-sepiolite nanocomposites, Appl. Clay Sci., 53 (2011) 181–187.

[19] I. Illisz, A. Dombi, K. Mogyorosi, I. Dekany, Photocatalytic water treatment with different TiO_2 nanoparticles and hydrophilic/hydrophobic layer silicate adsorbents, Colloids Surf. A, 230 (2004) 89–97.

[20] M.N. Chong, V. Vimonses, S. Lei, B. Jin, C. Chow, C. Saint, Synthesis and characterization of novel titania impregnated kaolinite nano-photocatalyst, Micropor Mesopor Mater., 117 (2009) 233–242.

[21] D. Kibanova, M. Trejo, H. Destaillats, J. Cervini-Silva, Synthesis of hectorite-TiO_2 and kaolinite-TiO_2 nanocomposites with photocatalytic activity for the degradation of model air pollutants, Appl. Clay Sci., 42 (2009) 563–568.

[22] J. Henych, V. Stengl, Feasible synthesis of TiO_2 deposited on kaolin for photocatalytic applications, Clays Clay Miner., 61 (2013) 165–176.

[23] L. Bouna, B. Rhouta, F. Maury, A. Jada, F. Senocq, M.C. Lafont, Photocatalytic activity of TiO_2/stevensite nanocomposites for the removal of orange G from aqueous solutions, Clay Miner., 49 (2014) 417–428.

[24] T. Kaneko, M. Fujii, T. Kodama, Y. Kitayama, Synthesis of titania pillared mica in aqueous solution of acetic acid, J. Porous Mater., 8 (2001) 99–109.

[25] L. Bouna, B. Rhouta, M. Amjoud, F. Maury, M.C. Lafont, A. Jada, F. Senocq, L. Daoudi, Synthesis, characterization and photocatalytic activity of TiO_2 supported natural palygorskite microfibers, Appl. Clay Sci., 52 (2011) 301–311.

[26] B. Ohtani, Y. Ogawa, S. Nishimoto, Photocatalytic activity of amorphous-anatase mixture of titanium(IV) oxide particles suspended in aqueous solutions, J. Phys. Chem., B101 (1997) 3746–3752.

[27] D. Beydoun, R. Amal, G. Low, S. McEvoy, Role of nanoparticles in photocatalysis, J. Nanoparticle Res., 1 (1999) 439–458.

[28] T. Monecke, S. Kohler, R. Kleeberg, P.M. Herzig, J.B. Gemmell, Quantitative phase-analysis by the Rietveld method using X-ray powder-diffraction data: application to the study of alteration halos associated with volcanic-rock-hosted massive sulfide deposits, Can. Mineral., 39 (2001) 1617–1633.

[29] L.B. Mc Cusker, R.B. Von Dreele, D.E. Cox, D. Louer, P. Scardi, Rietveld refinement guidelines, J. Appl. Cryst., 32 (1999) 36–50.

[30] D.L. Bish, S.A. Howard, Quantitative phase analysis using the Rietveld method, J. Appl. Cryst., 21 (1988) 86–91.

[31] K. Ufer, H. Stanjek, G. Roth, R. Dohrmann, R. Kleeberg, S. Kaufhold, Quantitative phase analysis of bentonites by the Rietveld method, Clays Clay Miner., 56 (2008) 272–282.

[32] D. Dermatas, M.S. Dadachov, Rietveld quantification of montmorillonites in lead-contaminated soils, Appl. Clay Sci., 23 (2003) 245–255.

[33] A.G. De La Torre, S. Bruque, M.A.G. Aranda, Rietveld quantitative amorphous content analysis, J. Appl. Cryst., 34 (2001) 196–202.

[34] T.C. Santini, Application of the Rietveld refinement method for quantification of mineral concentrations in bauxite residues (alumina refining tailings), Int. J. Miner. Process., 139 (2015) 1–10.

[35] Y. Kitayama, T. Kodama, M. Abe, H. Shimotsuma, Y. Matsuda, Synthesis of titania pillared saponite in aqueous solution of acetic acid, J. Porous Mater., 5 (1998) 121–126.

[36] C. Ooka, H. Yoshida, K. Suzuki, T. Hattori, Highly hydrophobic TiO_2 pillared clay for photocatalytic degradation of organic compounds in water, Microporous Mesoporous Mater., 67 (2004) 143–150.

[37] K.I. Shimizu, T. Kaneko, T. Fujishima, T. Kodama, H. Yoshida, Y. Kitayama, Selective oxidation of liquid hydrocarbons over photoirradiated TiO_2 pillared clays, Appl. Catal. A, 225 (2002) 185–191.
[38] M. Kassir, Ph.D. Thesis, University of Lorraine, France, 2013.
[39] M. Yuan, J. Zhang, S. Yan, G. Luo, Q. Xu, X. Wang, C. Li, Effect of Nd_2O_3 addition on the surface phase of TiO_2 and photocatalytic activity studied by UV Raman spectroscopy, J. Alloys Compd., 509 (2011) 6227–6235.
[40] H. Lin, C.P. Huang, W. Li, C. Ni, S. Ismat Shah, Y.H. Tseng, Size dependency of nanocrystalline TiO_2 on its optical property and photocatalytic reactivity exemplified by 2-chlorophenol, Appl. Catal. B: Environ., 68 (2006) 1–11.
[41] M. Kassir, T. Roques-Carmes, T. Hamieh, J. Toufaily, M. Akil, O. Barres, F. Villiéras, Improvement of the photocatalytic activity of TiO_2 induced by organic pollutant enrichment at the surface of the organografted catalyst, Colloids Surf. A, 485 (2015) 73–83.
[42] Z. Bouberka, K.A. Benabbou, A. Khenifi, U. Maschke, Degradation by irradiation of an acid orange 7 on colloidal TiO_2/(LDHs), J. Photochem. Photobiol. A: Chem., 275 (2014) 21–29.
[43] C. Leodopoulos, D. Doulia, K. Gimouhopoulos, T.M. Triantis, Single and simultaneous adsorption of methyl orange and humic acid onto bentonite, Appl. Clay Sci., 70 (2012) 84–90.
[44] K. Inumaru, M. Murashima, T. Kasahara, S. Yamanaka, Enhanced photocatalytic decomposition of 4-nonylphenol by surface-organografted TiO_2: a combination of molecular selective adsorption and photocatalysis, Appl. Catal. B., 52 (2004) 275–280.
[45] T. Sakai, A. Da Loves, T. Okada, S. Mishima, Titania/C_nTAB nanoskeleton as adsorbent and photocatalyst for removal of alkylphenols dissolved in water, J. Hazard. Mater., 248 (2013) 487–495.
[46] Y.J. Zhang, L.C. Liu, D.P. Chen, Synthesis of CdS/bentonite nanocomposite powders for H_2 production by photocatalytic decomposition of water, Powder Technol., 241 (2013) 7–11.
[47] V. Rakic, N.Rajic, A. Dakovic, A. Auroux, The adsorption of salicylic acid and atenolol from aqueous solutions onto natural zeolites and clays: clinoptilolite, bentonite and kaolin, Micropor. Mesopor. Mater., 166 (2013) 185–194.

Supporting information

Supporting information S1: Zeta potential measurements

Supporting information S2: TiO_2 leaching from the clay

Supporting information S3: Quantification of TiO_2 content using XRD measurements: Validation of the method

Two kinds of TiO_2 nanoparticles were used for the implementation of the quantification analysis (XRD + Rietveld). On the one hand, Anatase 50 nm titanium dioxide particles were employed as simple model since the material was pure anatase. They were purchased from MKNano (MK Impex, Canada). On the other hand, it was also interesting to study a commonly used photocatalyst with a more complex crystallographic structure. To this aim, titanium dioxide powder P25 was employed since it remained the state of the art photocatalyst. It was supplied by Evonik-Degussa. The particle diameter, estimated by transmission electron microscopy (TEM), was approximately equal to 25–30 nm.

A preliminary set of simple experiments with "model" mixtures were performed in order to assess the feasibility of the Rietveld analysis for the quantification of the TiO_2 amounts. For this purpose, Anatase 50 nm and P25 titania were employed. Several TiO_2/bentonite mixtures were prepared with different titania proportions varying from 1 wt.% to 50 wt.%. For each sample, 1 g of clay was used while the titania amount ranged between 0.2–1 g in order to modulate the nanoparticle content. The mixing of the powder materials was performed manually, by the mean of a mortar, or by using a metallic grinder (FRITSCH AZM 170).

The knowledge of the crystal-structure of each phase present in the investigated samples appears useful for the fitting process in Topas program. For that reason, the XRD pattern of each compound has to be recorded separately in order to determine the crystallographic parameters of the titania and the clay. Fig. S4 displays the XRD pattern of the

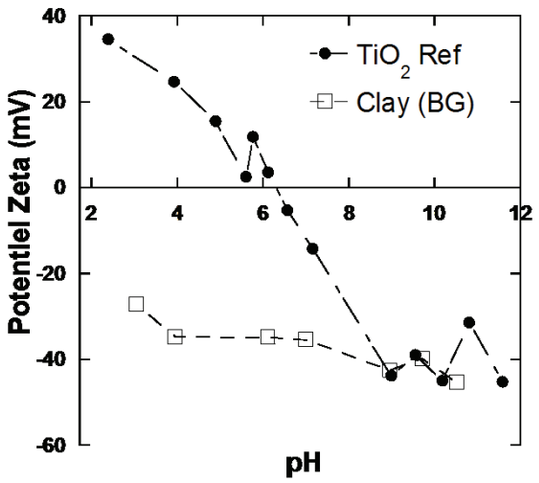

Fig. S1. Variation of the zeta potential as a function of pH of unsupported TiO_2 P25 ("TiO_2 Ref") and raw bentonite ("Clay (BG)").

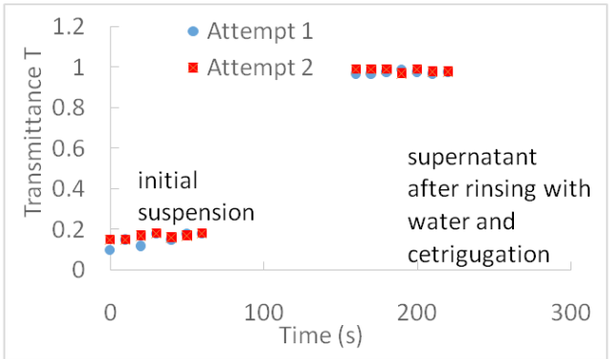

Fig. S2. Turbidimetric analysis (estimated by the transmission of light, ratio of transmitted light intensity: $T = I/I_0$). The data for the time range between 0 and 60 s correspond to the transmittance measured with the initial suspension while the data for the time range between 160 and 220 s correspond to the transmittance measured with the supernatant after the rinsing with water and centrifugation.

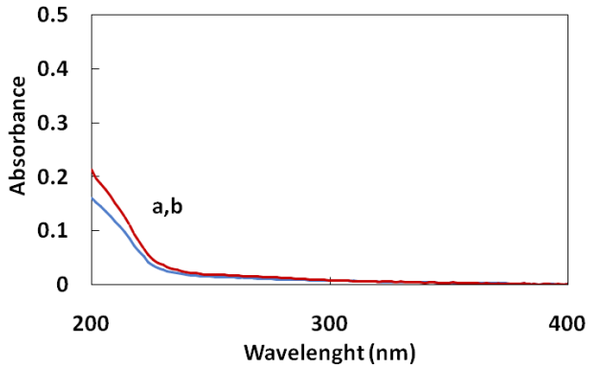

Fig. S3. UV/Visible absorption spectrum for the supernatant after the rinsing with water and centrifugation. (a) Attempt n°1 (blue) and (b) Attempt n°2 (red, dotted line).

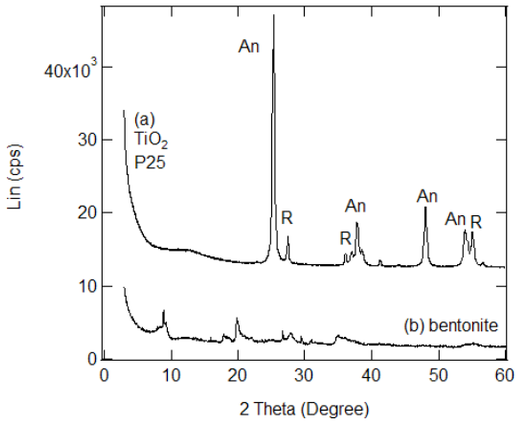

Fig. S4. X-ray diffraction patterns of (a) TiO_2 P25 and (b) bentonite after calcination at 450°C. The symbols "An" correspond to Anatase while "R" indicate Rutile structure. Parameter: Cu radiation.

TiO_2 P25 particles using a Cu radiation. The peaks located at 25.4°, 37.8°, 48.0°, 54.5° 2θ are assigned to the (101), (004), (200), (105) and (211) planes of the anatase phase, respectively (JCPDS 21-1272). Conversely, the peaks situated at 27.5°, 36.1°, 54.4° 2θ correspond to the (110), (101), (211) planes of the rutile phase, respectively (JCPDS 21-1276). The appearance of a relative small bump (around 10–20° 2θ) indicates the presence of non-negligible amount of amorphous phase.

The XRD pattern performed with a Co radiation is reported in the Fig. S5. It exhibits the same crystallographic phases which correspond to different 2θ positions than those obtained with Cu radiation. The peaks are shifted towards larger angles. The figure contains also the calculated X-ray diffraction pattern. From this output, it becomes possible to extract the weight percentages of anatase and rutile phases. The uptakes of anatase and rutile amount to 85 wt.% and 15 wt.%, respectively.

On the other hand, the XRD pattern for Anatase 50 nm titanium dioxide exhibits the characteristic reflections of anatase (Fig. S6, Co radiation). The diffraction peaks are detected at 29.5°, 44.3° and 56.1° in 2θ. They match well with the (101), (004) and (211) planes attributed to anatase. An additional large bump distributed in a relatively wide range of 2θ (ca. 5–15° in 2θ) suggests the presence of amorphous phase in the titania sample.

As far as the clay is concerned, the crystallographic analyze is performed with bentonite which has followed the same preparation pathway than those used in the composites (24 h in water and calcination at 450°C for 4 h). The XRD pattern obtained with the bentonite is reported in Fig. S7. It reveals several crystallographic phases including montmorillonite (d = 9.61 and d = 4.47 which correspond to 2θ = 9 and 25°) and calcite (d = 3.18 which corresponds to 2θ = 33°). It also contains some traces like quartz (d = 3.34 detected at 2θ = 31°), cristobalite, dolomite, illite, and albite. It appears also that the calcination of the clay induces a significant change in the position of the reflection basal peak corresponding to the basal spacing (Fig. S7). The diminution of the basal spacing from 12.46 Å (dry bentonite) to 9.61 Å for calcinated clay is observed. The

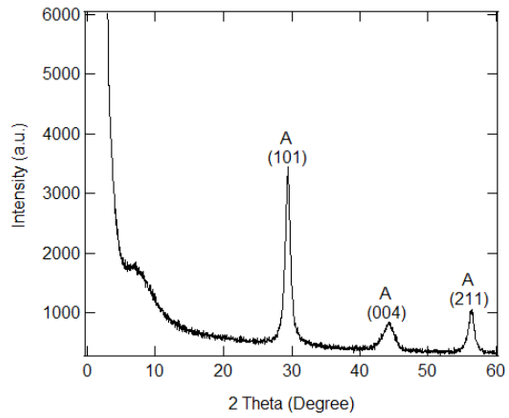

Fig. S6. X-ray diffraction pattern of Anatase 50 nm titanium dioxide particles. The symbols "A" correspond to Anatase. Parameter: Co radiation.

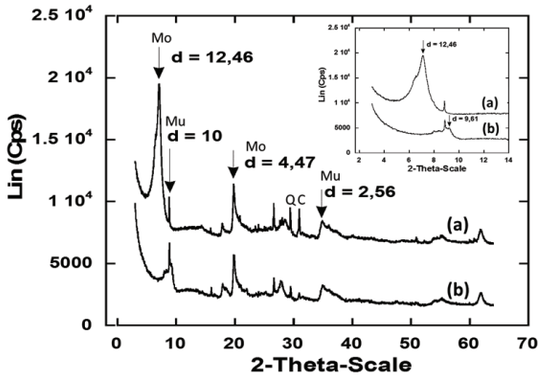

Fig. S7. Comparison of the X-ray diffraction patterns of (a) raw and (b) calcinated bentonite. The inset shows the reflection basal peak of the clay (a) before and (b) after calcination. Parameter: Cu radiation. The symbols "Mo" correspond to montmorillonite, "Mu" indicates muscovite, "Q" denotes quartz while the symbol "C" is related to calcite phase.

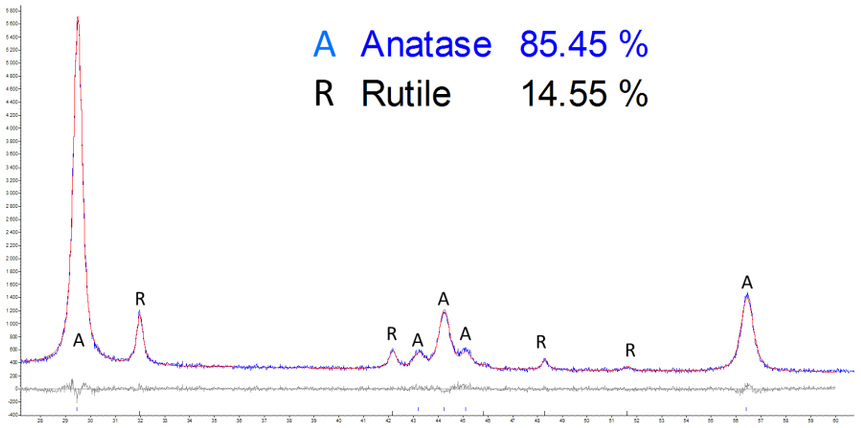

Fig. S5. Measured and calculated (using TOPAS 4.2.) X-ray diffraction patterns of TiO_2 P25. The purple line corresponds to the measured XRD pattern, the red smooth line represents the calculated XRD pattern, while the grey solid line below represents the difference curve between the measured and the calculated XRD patterns. Parameter: Co radiation. The mass fractions of anatase and rutile are indicated in the figure.

reduction of the basal spacing is attributed to the loss of partial inter-lamellar water which leads to dehydrated bentonite.

Experiments are carried out to validate the titania quantification approach in the case of TiO_2/bentonite mixtures. Fig. S8 shows an example of measured and calculated X-ray diffraction patterns of a P25 TiO_2/bentonite mixture in an experimental case that is quite typical and which has been selected to illustrate the method. The fit accounts for the majority of the data points and the various peaks (positions, shapes and intensities) are well reproduced. It takes into account all the peaks of the titania and the bentonite. From the fit, the amount of anatase, rutile and clay are extracted. In the case of Anatase 50 nm TiO_2, the titania content is equal to the weight percentage of anatase. On the contrary, for P25 titanium dioxide, the TiO_2 amount is calculated as the sum of the weight percentages of anatase and rutile. For the bentonite content, the weight percentage of clay is equal to the sum of the weight fractions of all the crystallographic phases except those of rutile and anatase.

We check the validity of the Rietveld approach by comparing the prepared and calculated percentages of titania for a variety of experimental conditions. The type of radiation (CuKα and CoKα radiations), the concentration and the nature of TiO_2 (P25 and Anatase 50 nm), the type of mixing of the powders, and the scanning range of 2θ were varied. Two series of experiments were performed with P25 TiO_2/bentonite mixtures to estimate the effect of the RX radiation: the first one using Co radiation (Fig. S9a) while the second one employed Cu radiation (Fig. S9b). Another series were performed, at constant Cu source of irradiation, to isolate the effect of the 2θ scanning range for P25/bentonite mixtures (Figs. S9b,c) and anatase/bentonite systems (Figs. S9d,e). It is also possible to evaluate the effect of the type of mixing and the nature of the titania particles. For each series of experiment, the calculated weight percentages of TiO_2 are plotted against the prepared weight percentages of titania. The results are depicted in Fig. S9. For each system, the data points fall on a single line indicating that the calculated titania uptake increases linearly with the prepared amount of TiO_2. With respect to a perfect correlation, the slope would be equal to 1. The slopes of the straight lines range between 0.94 and 1.07. They remain within the confidence range of the measurements. In addition, the majority of the linear regression coefficients remain better than 0.99. Nevertheless, the lower regression coefficient obtained with the data of the Fig. S9a ($R^2 = 0.96$) is mainly attributed to the large deviation visible for one value. The linear regression coefficient in the absence of this data becomes equal to 0.99. To summarize, the satisfactory agreement between the proposed Rietveld approach and the prepared data for a large range of titania and experimental conditions is a very strong argument in favor of the proposed method. It does also validate the analytical procedure. Nevertheless, some minor difference in the weight percentages of TiO_2 can be recognized. The general deviation is around 1–4 wt.%. This discrepancy might be caused by the small inhomogeneities in the sample which yield incorrect abundance of phases. In addition, the effects of amorphous components, preferred orientation and microabsorption are known to affect the precision of the Rietveld refinement for titania and clay. Nevertheless, we consider that the observed weak disagreement between experimental and simulated data comes mainly from the samples preparation. Actually, the processes of sieving and grinding induce drifts of the composites composition. Interestingly, the straight lines in Fig. S9 do not pass through the origin since the values of the intercept point are ranging from –0.70 to –1.65. This is due to the presence of amorphous phase in the titania materials. Recall that the Rietveld analysis is based on the quantification of the crystallized phases and does not take into account of the amorphous phase.

In addition, the Fig. S10 displays the full X-ray diffraction pattern of sol-gel TiO_2/bentonite composite (3-46° 2θ range) in order to reveal the layered structure of the bentonite in the composite.

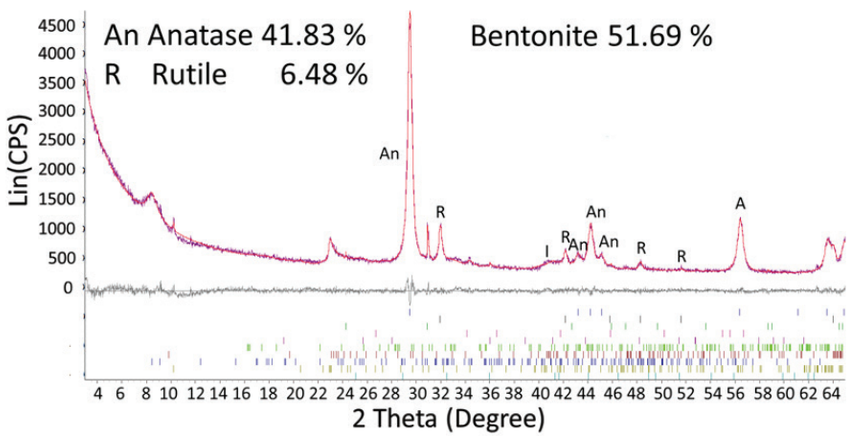

Fig. S8. Measured and calculated (using TOPAS 4.2.) X-ray diffraction patterns of TiO_2/bentonite. The purple line corresponds to the measured XRD pattern, the red smooth line represents the calculated XRD pattern, while the grey solid line below represents the difference curve between the measured and the calculated XRD patterns. The initial mixture contains 1 g of P25 titania and 1 g of clay. The mixing of the powders was carried out manually. Parameter: Co radiation.

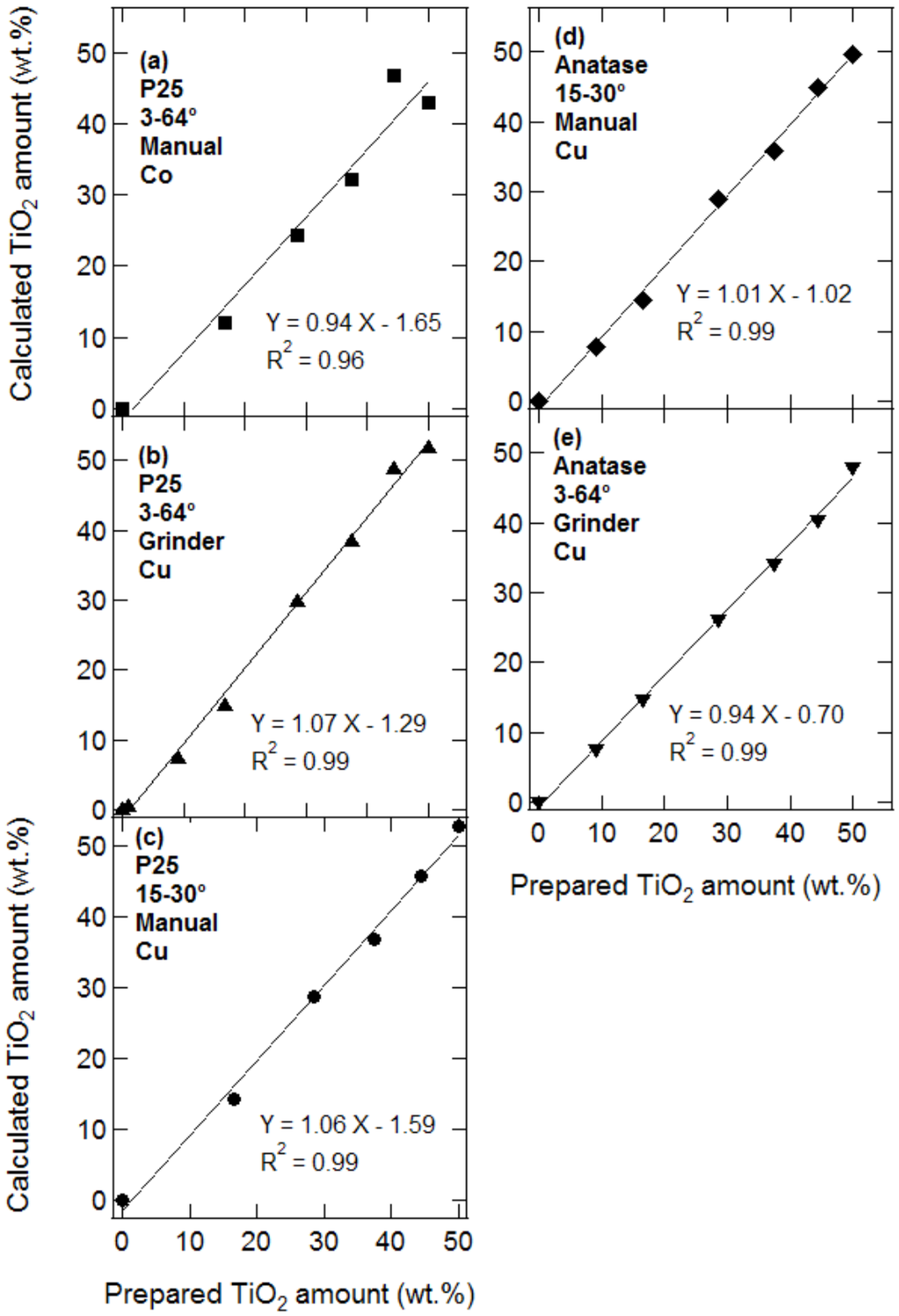

Fig. S9. Comparison between the prepared and calculated weight percentages of titania incorporated onto the clay. Plot of the calculated TiO_2 amount (from the diffractogram pattern and Rietveld analysis) versus the prepared titania content (prepared mixtures with a known amount of titania) for a variety of experimental conditions: (a) P25 TiO_2, manual mixing, Co radiation, 3–64° 2θ range; (b) P25 TiO_2, metallic grinder, Cu radiation, 3–64° 2θ range; (c) P25 TiO_2, manual mixing, Cu radiation, 15–30° 2θ range; (d) Anatase 50 nm TiO_2, manual mixing, Cu radiation, 15–30° 2θ range; (e) Anatase 50 nm TiO_2, metallic grinder, Cu radiation, 3–64° 2θ range. The lines represent the best linear fits.

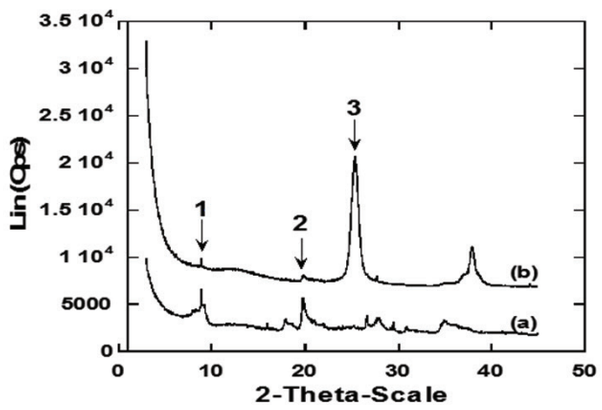

Fig. S10. X-ray diffraction patterns of (a) the raw bentonite and (b) a sol-gel TiO_2/bentonite sample fabricated with an initial mass of titanium tetraisopropoxide (IPPT) of 15.7 g. Parameter: Cu radiation.

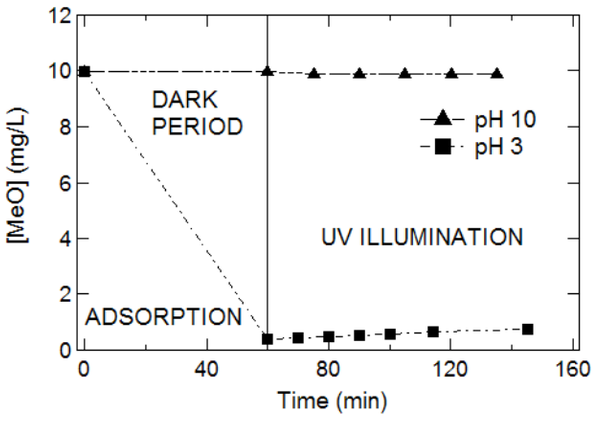

Fig. S11. Adsorption and photocatalytic degradation of methyl orange (MeO) by raw bentonite at different pH.

Supporting information S4: Adsorption and photocatalytic degradation of methyl orange by raw bentonite at different pH

Supporting information S5: XRF Analysis

Supporting information S6: Band gap determination from UV/visible spectra

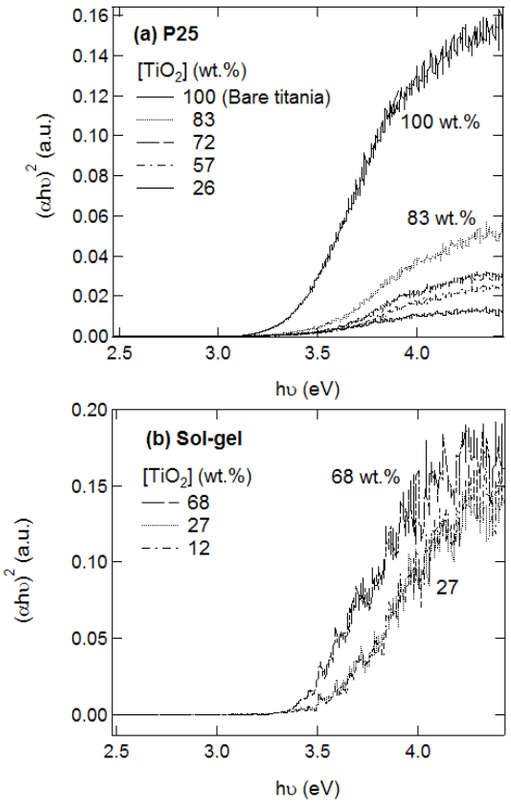

Fig. S12. $(ah\upsilon)^2$ as a function of the photon energy ($h\upsilon$) for TiO_2/bentonite composites.

Table S1
XRF analysis of the TiO_2/bentonite composites. The samples denoted "P25 1" and "P25 2" contained initial amounts of P25 titania in solution of 54 wt.% and 88 wt.%, respectively relative to the mass of bentonite. The samples named "Sol-gel 1" and "Sol-gel 2" are prepared with initial masses of IPPT in solution (relative to the mass of water) of 10 wt.% and 15.7 wt.%

Sample/Oxides (wt. %)	SiO_2	Al_2O_3	Fe_2O_3	TiO_2	MnO	MgO	CaO	Na_2O	FeO	K_2O
P25 1	16.1	5.8	2.7	54.2	0.09	1.2	0.09	18.3	1	0.27
P25 2	3.9	1.4	0.6	88.2	0.02	0.4	0.02	4.7	0.4	0.07
Sol-gel 1	20.1	7.2	3.3	42.1	0.11	1.5	0.18	23.5	1.5	0.35
Sol-gel 2	12.3	4.4	2.1	64.5	0.07	0.9	0.09	14.5	0.8	0.22